haematologica
Journal of the Ferrata Storti Foundation

Deep immunophenotypic dissection and clinical impact of T cells in the follicular lymphoma microenvironment

by Sary El Daker, David Qualls, Andriy Derkach, Samida Beqaj, Leonardo Boiocchi, Venkatraman Seshan, Jeeyeon Baik, Menglei Zhu, Gilles Salles, Ahmet Dogan, Mikhail Roshal and Pallavi Galera

Received: August 2, 2024.
Accepted: January 20, 2025.

Citation: Sary El Daker, David Qualls, Andriy Derkach, Samida Beqaj, Leonardo Boiocchi, Venkatraman Seshan, Jeeyeon Baik, Menglei Zhu, Gilles Salles, Ahmet Dogan, Mikhail Roshal and Pallavi Galera. Deep immunophenotypic dissection and clinical impact of T cells in the follicular lymphoma microenvironment.
Haematologica. 2025 Feb 6. doi: 10.3324/haematol.2024.286383 [Epub ahead of print]

Publisher's Disclaimer.
E-publishing ahead of print is increasingly important for the rapid dissemination of science. Haematologica is, therefore, E-publishing PDF files of an early version of manuscripts that have completed a regular peer review and have been accepted for publication.
E-publishing of this PDF file has been approved by the authors.
After having E-published Ahead of Print, manuscripts will then undergo technical and English editing, typesetting, proof correction and be presented for the authors' final approval; the final version of the manuscript will then appear in a regular issue of the journal.
All legal disclaimers that apply to the journal also pertain to this production process.

Deep immunophenotypic dissection and clinical impact of T cells in the follicular lymphoma microenvironment

Sary El Daker[1], David Qualls[2], Andriy Derkach[3], Samida Beqaj[1], Leonardo Boiocchi[1], Venkatraman Seshan[3], Jeeyeon Baik[1], Menglei Zhu[1], Gilles Salles[2], Ahmet Dogan[1], Mikhail Roshal[1], Pallavi Galera[1].

[1] Hematopathology Service, Department of Pathology and Laboratory Medicine*

[2] Lymphoma Service, Department of Medicine

[3] Department of Epidemiology and Biostatistics

* A member of the imCORE Network

Memorial Sloan Kettering Cancer Center, New York, NY, USA

Running title: Follicular Lymphoma T-cell Microenvironment

Corresponding author:
Dr. Pallavi Galera, MD
Department of Pathology and Laboratory Medicine, Memorial Sloan Kettering Cancer Center,
1275 York Avenue, New York, NY 10065
Email: GaleraP@mskcc.org
Tel: +1212-639-2596

Funding:
This study was supported by the imCORE Network/Genentech Inc.

Authorship contributions:
S.E.D., J.B. and P.G. identified patients. P.G., M.R. and A.Dogan. reviewed pathology. S.E.D. performed flow cytometric analysis and plotted figures. S.E.D, P.G., M.Z., M.R. and A.Dogan. analyzed and reviewed the flow cytometric data. D.Q. collected clinical data and reviewed it with G.S. S.B. and L.B. performed multiplex immunofluorescence assay. S.B., L.B. and P.G. analyzed and reviewed the multiplex immunofluorescence assay. V.S. and A.Derkach. performed statistical analysis. A.Dogan. and M.R. supervised the project. S.E.D, P.G. and D.Q. wrote and all authors provided critical review and revision of each manuscript draft and provided approval for submission of the final draft.

Conflict of Interest:
M.Z. is on the advisory board in Leica biosystems. M.R. is on the scientific advisory board in Auron Pharmaceutical for which he received equity support. He receives research funding from Celularity, Roche-Genentech, Beat AML and NGM, travel fund from BD Biosciences and does compensate advising for Syros. P.G. has received research support from Paige.AI. G.S. provided consultancy and/or received honoraria from AbbVie, Allogene, Beigene, BMS/Celgene, Debiopharm, Epizyme, Genentech/Roche, Genmab, Incyte, Ipsen, Janssen, Kite-Gilead, Loxo, Miltneiy, MorphoSys, Novartis, Rapt, Regeneron, Takeda, and Velosbio and was also funded in part through the NIH/NCI Cancer Center support grant P30 CA008748. A.Dogan. received honoraria and consulting or advisory role fees from Roche, Corvus Pharmaceuticals, Physicians' Education Resource, Seattle Genetics, Peerview Institute, Pharmacyclics, Celgene, Novartis, Loxo, Takeda, and EUSAPharma; and research grants from National Cancer Institute and Roche-Genentech.

Data-sharing statement:
Original data can be shared upon request by contacting the corresponding author.

Part of this work was presented at American Society of Hematopathology Annual meeting 2021, USCAP 111th Annual Meeting 2022, European Association for Hematopathology workshop 2022 and American Society of Hematopathology Annual meeting 2022.

Abstract word count: 249
Main text word count: 3930
Figures: 6
Tables: 2
Supplementary Figures: 15 (1 PDF file)
Supplementary Tables: 9 (1 excel file)
References: 47

ABSTRACT

Follicular lymphoma (FL) is an indolent B cell lymphoma with a heterogenous disease course, and patients may not require immediate treatment upon diagnosis. Scrutiny of its microenvironment may provide key insights into lymphomagenesis and enhancement of therapeutic options.

We analyzed the T-cell composition of a large, well-annotated follicular hyperplasia (FH; n=43) cohort utilizing standardized high dimensionality flow cytometry (>150,000 cells analyzed/sample) and a novel reproducible analytical pipeline leading to identification of even minor T-cell subsets. This baseline reference set was compared to prospectively collected FL samples (n=91) from untreated patients (FL-UT) and patients with relapsed/refractory disease (FL-RR). Compared to FH, both FL-UT and FL-RR specimens exhibited depletion of CD4+ & CD8+ naïve subsets and were characterized by an immune suppressive microenvironment enriched in specific inhibitory T-cells, along with exhausted memory T-cells overexpressing varying combinations of immune checkpoint receptors. FL specimens showed enrichment of T follicular regulatory cells (TFR) and two highly suppressive regulatory T-cell (T-reg) populations expressing TIGIT and CTLA4 (TC) and PD1, TIGIT, CTLA4, and TIM3 (PTCTi). FL-UT cases with either increased T-reg TC or increased T follicular helper cells (TFH) showed reduced time to first treatment (</= 3 months).

Our study suggests that changes in the balance between TFR, T-Reg and TFH may lead to greater tumor growth and identifies factors that are associated with earlier time to treatment in FL-UT. We also identified specific combinations of immune checkpoint receptors that may be used to target specific inhibitory T-cell subsets and regulatory cells in FL to increase anti-tumor immune response.

INTRODUCTION

Follicular lymphoma (FL) is the most common type of indolent non-Hodgkin lymphoma.[1] Despite improvements in therapy, FL remains incurable with standard therapy, and most patients have multiple relapses.[2] The disease course is heterogeneous, with a subset of patients having early progression and transformation to aggressive B-cell lymphomas, while the others have indolent disease and do not require immediate treatment. Several markers and indices have been studied in pursuit of better prognostication of FL, though these are not routinely used to guide management.[3-7] Therefore, improvements in prognostic and therapeutic approaches are needed.

Prior studies have suggested that the nonmalignant immune cells present in the FL tumor microenvironment (TME) may predict survival and patient outcome.[8-16] The neoplastic B-cells in FL are dependent on the dynamic bidirectional communication with their TME for their proliferation and survival .[15,17-19] Dissection of TME composition provides valuable insight into lymphomagenesis, better prognostication, and enhancement of therapeutic options. However, FL TME has been partially studied employing only a limited number of samples. Comprehensive and large scaled studies characterizing FL TME utilizing a robust, reproducible approach for analyzing the multidimensional data are currently lacking. Furthermore, studies elucidating the dynamics of TME change during lymphoma treatment and in relapse settings are crucial.

It is also essential to have extensive repositories of normal/ reactive tissue to serve as a basis for future discoveries and translational cancer research. Reactive lymph nodes (LNs) reveal structural and functional differences depending on their site of drainage.[20] Thus, large scale studies describing and defining the T-cell repertoire in normal reactive LNs are required. To address this, we created a highly detailed T-cell subset library of reactive LNs from a wide range of sites. Since LNs with follicular hyperplasia (FH) are physiologically the closest comparator group for FL, a cohort of FH cases was analyzed as the baseline reference set. The second aim of the study was to compare this baseline reference set with tumor infiltrating T-cell subsets in FL, including untreated patients (FL-UT) and patients with relapsed/refractory disease (FL-RR), to construe FL TME and its evolution with treatment. Flow cytometry is a powerful and reproducible method for single-cell analysis. Thus, we utilized a robust standardized high dimensionality flow cytometry approach along with a novel reproducible analytical pipeline.

METHODS

1. Case selection and retrospective clinical data collection

A cohort of LN samples displaying immunophenotype consistent with FH, defined as at least 10% of B-cells showing germinal center B-cell phenotype with intermediate CD10 and CD38 expression, was obtained from the Memorial Sloan Kettering Cancer Center flow cytometry laboratory database. In cases with concurrent histologic specimens, FH was further verified by morphology. A second cohort of FL cases was obtained through integrated flow cytometric and morphologic analysis which was independently reverified by P.G., M.R., and A.Dogan. according to the WHO Classification of Tumors of Hematopoietic and Lymphoid Tissues (2017).[1] The neoplastic B-cells were identified by flow cytometry as a discrete B-cell population with an aberrant immunophenotype including dim CD19, CD10, dim/negative CD38, dim CD20, dim/intermediate CD45 and light chain restriction. Clinical data was retrospectively collected for all FL patients including basic demographic data, clinical characteristics, treatment, and outcome data. The Institutional Review Board of Memorial Sloan Kettering Cancer Center approved the study.

2. Antibodies

Two panels (16 antigens/9 colors; Table S1) were utilized for the initial characterization and quantification of the B-cells, T-cells, and natural killer (NK) cells by flow cytometry. In addition, 2 research panels (23 antigens/18 colors) were developed for this study. Research panel I was developed to identify the T-cell subsets (CD4, CD8 and CD4/CD8 double negative T-cells), their activation state (naïve, central memory, effector memory, effector, T-memory stem cells), and their immune checkpoint expression (TIGIT, TIM3, PD-1, CD96, LAG3, CTLA4, CD73). Research panel II was used to further characterize the CD4+ subsets, identified through panel I, with chemokine receptors CXCR5, CXCR3, CCR6, and CCR10. Each panel was validated by performing Fluorescence Minus One, single-stain, and precision tests. Samples were acquired on BD LSR Fortessa X-20 flow cytometer with 18 detectors and BD FACSCanto flow cytometer (for details see supplementary methods). IHC studies (Table S2) were performed for diagnostic purposes, and additional stains were performed to study the topographic distribution of various T-cell subsets on 10 FH, 8 FL-UT and 5 FL-RR excisional LN specimens. In addition, multiplex immunofluorescence (MxIF) assay was performed targeting CD3, CD20, CD4, FoxP3, PD-1 and BCL-6 antigens (Table S3) on 3 excisional specimens each of FH, FL-UT and FL-RR cases.

3. Analytical pipeline and T-cell subsets

Research Panel I was analyzed using a new analytical pipeline that was specifically designed to reduce human bias during cluster identification (Figure S1). Briefly, T-cells were identified using CD3 and scatter parameters and used as input for the analytical pipeline. To minimize technical variation in sample acquisition over time we used the R-based algorithm GaussNorm.[21] To avoid computational artifacts due to misreading of high-density regions, the following channels were excluded from the normalization: BV480-CCR7, APC-CTLA4, BUV395-TIGIT, and BV605-PD1. 8000 CD3+ events from each sample were concatenated, and the file generated (containing both FH and FL specimens) was used to identify the T-cell subsets by combining a dimensionality reduction technique (UMAP)[22] with an unsupervised clustering algorithm (FlowSOM)[23] using the OMIQ software from Dotmatics. Expert manual sub-clustering was performed to refine phenotypes that showed excessive heterogeneity.

Utilizing data from all the 134 samples (43 FH and 91 FL) we identified 13 CD4+ and 6 CD8+ T-cell subsets through this pipeline (Figure 1). Each population was characterized using a previously well-described phenotype reflecting physiological functions.[24,25] Their detailed phenotypes are illustrated in Figure 1C.

The phenotype observed in the TFR, TFH and T-reg populations with Research panel I, was reproduced through manual gating using the common markers in Research Panel II for further characterization.

RESULTS

1. Cohort clinicopathologic characteristics (Table 1)

Forty-three FH and 91 FL cases including 54 FL-UT and 37 FL-RR were obtained between January 2019 and December 2020. Patient characteristics are summarized in Table 1. In the FL-UT cohort most of the cases (43 of 54) were diagnosed as grade 1-2, with 9 grade 3A and 2 grade 3B FL. At a median follow-up of 2.4 years, 36 patients had initiated treatment for FL at a median of 31 days (interquartile range, 21 – 89) after the biopsy, and 10 patients experienced disease progression within 24 months of first therapy initiation (POD24). The median progression-free survival (PFS) from the time of front-line therapy in treated patients was 2.25 years. Transformation to diffuse large B-cell lymphoma (DLBCL) was seen in 4 patients.

In the FL-RR cohort grade 1-2 was observed in 31, grade 3A in 5, and grade 3B FL in 1 of the 37 samples. Prior to biopsy, FL-RR cohort patients had received a median of 1 (range, 1-6) prior lines of therapy, including anti-CD20 monoclonal antibody-containing therapy in 34 patients and chemotherapy in 28 patients, with anthracycline-containing regimens in 21 patients. POD24 had occurred in 49% of patients. Transformation to DLBCL, with treatment and complete remission of aggressive disease, had previously occurred in 9 patients. The median time from last treatment to biopsy time was 1.8 years (range, 0.002-12.5) with 7 patients receiving treatment within last 1 year of sampling. All but 1 patient (n = 34) in the FL-RR cohort received subsequent therapy, a median of 30 days (IQR 20-59) after biopsy. The median PFS after this new line of treatment initiation was 10.1 months, with 16 patients having POD within 24 months of treatment initiation and 3 having subsequent transformation after biopsy.

2. Characterization of the T-cell repertoire in FH LN specimens

To create a baseline, we first analyzed the T-cell subset distribution in the FH cohort (Figure 1). Naïve cells (CD45RO-CCR7+) were the most represented subsets in both CD4 and CD8 compartments (28.2% and 6.2% of CD3+ T-cells, respectively), followed by memory cells not expressing any inhibitory immune checkpoint receptors namely CD4+ central memory (CM; CD45RO+CCR7dim+), and a distinct CD8+ subset showing phenotypic overlap between central memory and effector memory T-cells (CD45RO+, CCR7dim+/-, CD95+, CD73dim+) designated as CM/EM. In the CD4 compartment, high numbers of T-follicular helper cells (TFH) expressing bright PD1 along with TIGIT and CTLA4 were also noted. While the T-follicular regulatory cells (TFR) expressing FoxP3, dim/intermediate PD1, and dim/negative CD25 were rare. Most of the regulatory T-cells (T-reg; CD4+FoxP3+CD25+) showed a non-inhibitory phenotype, characterized by a dim/negative expression of CTLA-4 and CD45RO (T-reg Naïve and T-reg EM). A small subset of FH patients (n=9) had a prior history of chemo/radiotherapy for other non-FL cancers. Comparison of the T-cell repertoire between patients with no history of prior chemo/radiotherapy and patients with prior therapy revealed no significant differences except for two small CD4+ subsets (naïve T-regs and EM T-regs; p value ≤ 0.05; Figure S2). No significant differences were observed on evaluating the T-cell subset distribution among the different sites in FH LNs (Figure S3).

3. FL TME shows significant difference from FH T-cell repertoire (Table 2)

From the analysis performed on the initial characterization flow cytometry panel (Table S4) we observed a significant decrease in the number of NK-cells, T-cells and as expected non-neoplastic B-cells while the B:T ratio was significantly higher in both the FL cohorts, in comparison to FH specimens (Figure S4).

In contrast to FH specimens, FL specimens revealed a significant depletion of naïve T-cells, in both CD4 and CD8 subsets (Figure 1A).

3.1 FL specimens show an immune suppressive microenvironment

FL specimens were enriched in 2 subsets of activated T-regs: one expressing TIGIT, CTLA4 (T-reg TC; p-value 0.001 for both FL-UT and FL-RR) and the other expressing PD1, TIGIT, CTLA4, and TIM3 (T-reg PTCTi; p-value 0.001 for both FL-UT and FL-RR; Figure 2A-D). T-reg subsets expressing various immune checkpoint receptors have previously shown to be highly suppressive.[26-29] With the expansion of these highly suppressive T-reg subsets (T-reg TC and T-reg PTCTi) a concomitant reduction in CD4 effector cells was noted in the FL specimens (Figure 1A, Table 2). This was further accentuated in the FL-RR cohort with CD4 effector cells (Figure S5).

In addition, the FL samples also revealed an expansion in CD4+ populations known to be responsible for germinal center formation, maturation, and maintenance, namely the TFH and TFR. Both these subsets were present at a higher frequency in the FL samples (FL-UT; p-value 0.001 for both TFH & TFR and FL-RR; p-value 0.002 for TFH and 0.001 for TFR) compared to FH samples (Figure 2A-D).

Both T-regs and TFR populations show phenotypic overlap with the expression of CD45RO, FoxP3, CTLA4, and TIGIT; however, were distinguished based on the differential expression of CD25 (brighter on T-regs; Figure 1C and 2C) and CXCR5 evaluated on research panel II (predominantly positive on TFR; Figure 2D and Figure S6).

3.2 FL T-cell microenvironment shows an expansion of exhausted memory T-cells

In addition to the expansion of the inhibitory subsets of T-regs and TFR, FL specimens showed a marked increase in specific exhausted T-cell subsets (Figure 3). The concentration of CD4 EM expressing PD1, TIGIT, CTLA4 and TIM3 (EM PTCTi) was two-fold higher in both FL cohorts in comparison to FH specimens (Figure 3A). However, the frequency of CD4 EM expressing PD1, TIGIT (EM PT) and PD1, TIGIT, CTLA4 (EM PTC) did not change among the cohorts. In contrast, CD8 EM were characterized by the expansion of double positive PD1, TIGIT cells (EM PT), triple positive PD1, TIGIT, CTLA4 cells (CD8 EM PTC) and cells expressing bright TIM3 in addition to the other 3 inhibitory receptors (EM PTCTi) (Figure 3B).

4. Alterations in FL-RR microenvironment in comparison to FL-UT

An expansion of TFH and TFR populations was observed in both FL-UT and FL-RR cases. However, the FL-RR cases revealed a significantly greater expansion of the TFR compared to FL-UT specimens (Figure S7; p-value=0.018). In contrast, naïve T-regs, known to be resistant to apoptosis induction and less immunosuppressive than memory T-regs, were reduced in FL-RR in comparison to both FH and FL-UT samples (Figure S7; p-value=0.04).

5. Topographic evaluation of T-cell microenvironment of FH, FL-UT and FL-RR

The spatial distribution of the various T-cell subsets was examined using MxIF assay and IHC studies. In the FH samples, MxIF studies revealed the presence of CD3+CD4+PD1+BCL6+ TFH cells within the germinal centers, polarized predominantly to the light zone (Figure 4A). Corroborating these findings, the IHC studies also revealed CD4+ PD1 brightly+ TFH cells (Figure S8) in a similar distribution, that were also positive for ICOS, CTLA4, and TIGIT. Few CD3+CD4+FoxP3+PD1negative T-regs (additionally positive for CD25 by IHC) were evenly distributed in the sinusoids and medullary cords. Rare cases revealed increased T-reg cells. On further investigation, these were found to have recent histories of carcinoma (lung and breast).

Similar to FH LN specimens, these populations were visualized on FL LN tissue sections utilizing MxIF and IHCs. The TFH cells were seen within the neoplastic follicles. Cells expressing CD3, CD4, FoxP3, PD1 (dim), BCL6 and ICOS were identified as TFR cells and were seen both within and surrounding the neoplastic follicles (Figure 4A and Figure S8). These studies also confirmed the presence of a higher number of TFR cells in FL-RR specimens (Figure 4A and Figure S8).

The images were further analyzed using the image analysis platform HALO and the percentage of TFH and TFR as % of total CD3 positive T-cells was calculated. On performing linear regression analysis for these 2 subpopulations evaluated by MxIF vs. flow cytometry, a strong correlation was found for both the populations, with a coefficient of determination (R-squared) equal to 0.93 for TFR and 0.8 for TFH subpopulations (Figure 4B).

6. Immune suppressive microenvironment in FL is associated with earlier initiation of therapy in FL-UT

The association between these immune suppressive populations (T-reg TC, T-reg PTCTi, TFR) & TFH and various pathologic and clinical parameters was examined. First, we analyzed the time to first treatment in FL-UT cohort as a discrete clinically defined time point; ≤3 months, >3 months and patients never receiving any treatment during follow-up. This analysis revealed that the presence of a higher percentage of T-reg TC cells and TFH cells were associated with earlier initiation of therapy in the FL-UT cohort (Figure 5A and 5B), while T-reg PTCTi and TFR cells did not show an association with time to first treatment (Figure S9). After adjusting for age, stage and FLIPI scores these results remained significant for the T-reg TC population but not for TFH population (Tables S5 and S6).

Employing a different approach, we performed maximally selected rank statistics on the FL-UT cases and estimated optimal cutoff thresholds for T-reg TC and TFH percentages (2.7% and 4.79% of WBC, respectively) (Figure S10). Utilizing these cutoff thresholds, the time to event analysis revealed that patients with T-reg TC and TFH percentages above the cutoff thresholds had significantly shorter time to first treatment (Figure 5C and 5D). On a multivariate analysis, confounding factors of age, stage and FLIPI scores did not change the significance or magnitude of results for both T-reg TC and TFH populations (Tables S7 and S8).

There was no association between the frequency of T-regs, TFH, or TFR cells and other clinicopathologic parameters namely the tumor grade (grade 1-2 versus grade 3A/B), lymphoma stage, anatomic site, patient age (>/< 60 years), or FLIPI (low/intermediate versus high) (Figure S11) in both the FL cohorts.

7. Unsupervised hierarchical clustering based on T-cell subsets distinguished FH specimens from FL specimens and identified a unique subset of FL cases

To further explore the distribution of various T-cell subsets in an unbiased manner, we took an orthogonal approach and performed unsupervised hierarchical clustering based on T-cell subsets as a percentage of WBCs. This revealed three distinct clusters (Figure 6). Clusters #1 and #2 were enriched in FL specimens without clear separation between FL-UT and FL-RR specimens. However, FH specimens clustered separately as cluster #3 with 10 FL-UT being admixed in this cluster. The T-cell subsets driving the unsupervised hierarchal clustering were TFH, TFR, T-reg TC, and T-reg PTCTi, which were increased in clusters #1 and #2 (Figure S12), and CD4 naïve, CD4 CM, and CD4 effector cells, which were decreased in clusters #1 and #2 in comparison to cluster #3. A higher proportion of T-reg TC and TFR in cluster #2 (Figure S13) distinguished it from cluster #1.

Cluster #3 was enriched in FH specimens and showed an admixture of 10 FL-UT cases (FH-like FL cases). These “FH-like FL” cases had significantly fewer TFH, T-reg TC and T-reg PTCTi in comparison to other FL-UT cases present in clusters #1 and #2 (Figure S14). The pathologic features including the extent of involvement of the specimen (complete vs partial involvement), anatomic site, and tumor grade of these “FH-like FL” cases showed no significant differences compared to cluster #1 and #2 FL-UT cases. However, of the 8 “FH-like FL” cases having available clinical data, only 2 initiated therapy within 6 months from diagnosis (including one with stage 1 disease who received radiotherapy), as opposed to 26 out of 40 patients with FL-UT in the other two clusters. They also showed higher proportion of stage 1 disease (3 of 8 vs. 2 of 40) and no patients had a FILPI score of 4-5 (Table S9). Although, there was no significant difference in overall survival, the time to first treatment of the “FH-like FL” cases showed a trend towards longer treatment-free time intervals compared to FL-UT cases in clusters #1 and #2 (Figure S15).

DISCUSSION

This study is the first to combine computational algorithms with single-cell analysis to comprehensively characterize the T-cell composition of a large, well-annotated FH reference set from different anatomic sites. Using this extensive library as a baseline, we were able to examine the T-cell microenvironment of FL specimens, including untreated and previously treated relapsed/ refractory samples. This has important clinical implications as recent studies have highlighted the critical role of TME in the regulation of immune response and the efficacy of anti-tumor therapies. While blocking antibodies against immune checkpoint receptors have not shown much clinical efficacy in FL, these therapies alone or in combination with other therapies, have shown beneficial effect on other lymphoma subtypes.[30-32] Given the development of T-cell based therapies in FL, including chimeric antigen receptor T-cells and bispecific T-cell engaging antibodies, there is greater interest in understanding T-cell microenvironment which may be associated with outcome.[33-35]

In our study FL specimens revealed a significant depletion of both CD4 and CD8 naïve T-cells along with depletion of CD4 CM and CD4 effector cells. Yang et al.[36] reported a significantly lower number of naïve T-cells in FL specimens in comparison to tonsils and the frequency of naïve T-cells correlated with improved patient survival. They also reported that activated effector memory cells and naïve T-cells were highly represented in tonsil tissue. Another study indicated that a lack of intrafollicular activated CD4 CM T-cells predicted early clinical failure in newly diagnosed FL patients. [37]

We observed that FL specimens were characterized by an immune suppressive microenvironment enriched in inhibitory cells and exhausted memory cells. Two distinct CD4 inhibitory subsets were expanded in FL specimens: T-regs and TFR. T-regs repress the immune response targeting a wide range of immune cells, including lymphocytes, macrophages, and dendritic cells.[38] They are comprised of many cell states with specialized regulatory functions. Studies have shown that intra-tumoral T-regs are overrepresented in B cell lymphomas and suppress proliferation and cytokine production of infiltrating CD4+CD25- T-cells.[39] Here, we observed the expansion of two highly suppressive T-reg phenotypes: T-reg TC expressing CTLA4 and TIGIT and T-reg PTCTi expressing CTLA4, TIGIT, PD1 and TIM3. Several studies reveal that TIGIT+ T-regs can specifically suppress the pro-inflammatory Th1 and Th17 (but not Th2) immune response, while T-reg expressing TIM3 are specialized tissue-resident T-regs that accumulate in FL tissue in the early stages and promote neoplastic growth.[40,41] In keeping with these studies, our analysis revealed that a higher percentage of T-reg TC was associated with earlier initiation of therapy in previously untreated patients.

TFR is a distinct subset of CD4 T helper cells that express FoxP3, acquire a follicular phenotype, and migrate into germinal centers of the LNs, where they exert their specific regulatory role by modulating TFH number and functioning.[42-44] It has been postulated that the balance between TFH and TFR helps shape the humoral response, with TFH promoting the formation and maintenance of germinal centers in secondary lymphoid organs and TFR inhibiting B cell and TFH activation[42-44]. Both TFH and TFR populations were expanded in FL cases. Our data shows that in FL-UT cases, a higher percentage of TFH was associated with an earlier initiation of therapy. While both TFH and TFR compartments were expanded in FL, the FL-RR cases showed a further expansion of TFR compartment in comparison to FL-UT cases. This likely reflects a more immunosuppressive environment suggesting that a disequilibrium favoring TFR in the TFH/TFR balance may lead to tumor re-growth and possibly therapy-resistant disease in FL.

To further explore the clinical impact, we pursued optimal cutoff points for T-reg TC and TFH (2 subsets which were seen associated with earlier time to first treatment). These were 2.75% and 4.79% T-reg TC and TFH, respectively. At these cutoff percentages, the treatment naïve cases showed clear separation into cohorts requiring early treatment. However, our cohort of untreated patients with complete clinical data was comprised of 48 cases with limited clinical follow-up, limiting conclusions. Further expansion and longer-term follow-up may facilitate the creation of a more comprehensive predictive model including other T-cell subsets.

In line with prior studies,[15,45-47] we also observed a marked expansion of exhausted memory T-cells in FL, characterized by varying combinations of PD1, TIGIT, CTLA4 and TIM3. While effector memory cells co-expressing PD1, TIGIT and PD1, TIGIT, CTLA4, TIM3 were equally distributed and expanded in both CD4+ and CD8+ compartments, triple positive PD1, TIGIT, TIM3 and PD1, TIGIT, CTLA4 were specifically expanded only in the CD8 and CD4 compartments, respectively. Therefore, co-targeting the inhibitory receptors PD1 and TIM3, may be an effective strategy in FL to repristinate the CD8 effector functions and, at the same time, to promote the Th1 pro-inflammatory response by blocking Th1-specific T-regs.

Another unique finding of the current study is the clusters identified by unsupervised hierarchical clustering based on T-cell subsets. Despite being purely based on T-cell microenvironment, the clustering accurately differentiated FL from FH cases (clusters #1 and #2). Cluster #3, though enriched in FH cases, had 10 FL-UT cases we describe as "FH-like FL" cases. These "FH-like FL" cases were indistinguishable pathologically from the other FL-UT cases. However, on a closer review of their clinical characteristics, they showed a trend towards longer treatment-free time intervals compared to other FL-UT cases, identifying a potentially more indolent or early group of FL cases with a less disturbed microenvironment.

In summary, FL specimens showed an immune suppressive microenvironment enriched in activated T-regs, TFR, and exhausted memory T-cells. This immune suppressive microenvironment was found to be associated with an earlier initiation of therapy in newly diagnosed patients. Furthermore, our data indicate that the altered balance between TFH and TFR occurs in patients with recurrent disease, potentially reflecting a more tumor-prone or therapy-resistant environment. We also identified a specific combination of immune checkpoint receptors that may be used to target specific inhibitory T-cell subsets and regulatory cells in FL in an effort to increase anti-tumor immune response.

Our study provides an extensive, well-characterized library of the FH microenvironment and a robust framework for further investigations with larger study cohorts with longer follow-ups that may be helpful in creating a TME prognostic index for FL. Given that our study utilizes flow cytometry instead of sequencing-based techniques, it might be easily implemented in multiple centers with shorter processing time and lower cost.

REFERENCES

1. Swerdlow SH, Campo E, Harris NL, et al. WHO Classification of Tumours of Haematopoietic and Lymphoid Tissues. Lyon, France: International Agency for Research on Cancer (IARC). 2017.
2. Batlevi CL, Sha F, Alperovich A, et al. Follicular lymphoma in the modern era: survival, treatment outcomes, and identification of high-risk subgroups. Blood Cancer J. 2020;10(7):74.
3. Solal-Céligny P, Roy P, Colombat P, et al. Follicular lymphoma international prognostic index. Blood. 2004;104(5):1258-1265.
4. Federico M, Bellei M, Marcheselli L, et al. Follicular lymphoma international prognostic index 2: a new prognostic index for follicular lymphoma developed by the international follicular lymphoma prognostic factor project. J Clin Oncol. 2009;27(27):4555-4562.
5. Pastore A, Jurinovic V, Kridel R, et al. Integration of gene mutations in risk prognostication for patients receiving first-line immunochemotherapy for follicular lymphoma: a retrospective analysis of a prospective clinical trial and validation in a population-based registry. Lancet Oncol. 2015;16(9):1111-1122.
6. Bachy E, Maurer MJ, Habermann TM, et al. A simplified scoring system in de novo follicular lymphoma treated initially with immunochemotherapy. Blood. 2018;132(1):49-58.
7. Huet S, Tesson B, Jais JP, et al. A gene-expression profiling score for prediction of outcome in patients with follicular lymphoma: a retrospective training and validation analysis in three international cohorts. Lancet Oncol. 2018;19(4):549-561.
8. Dave SS, Wright G, Tan B, et al. Prediction of Survival in Follicular Lymphoma Based on Molecular Features of Tumor-Infiltrating Immune Cells. N Engl J Med. 2004;351(21):2159-2169.
9. Farinha P, Masoudi H, Skinnider BF, et al. Analysis of multiple biomarkers shows that lymphoma-associated macrophage (LAM) content is an independent predictor of survival in follicular lymphoma (FL). Blood. 2005;106(6):2169-2174.
10. Carreras J, Lopez-Guillermo A, Roncador G, et al. High numbers of tumor-infiltrating programmed cell death 1-positive regulatory lymphocytes are associated with improved overall survival in follicular lymphoma. J Clin Oncol. 2009;27(9):1470-1476.
11. Richendollar BG, Pohlman B, Elson P, Hsi ED. Follicular programmed death 1-positive lymphocytes in the tumor microenvironment are an independent prognostic factor in follicular lymphoma. Hum Pathol. 2011;42(4):552-557.
12. Laurent C, Müller S, Do C, et al. Distribution, function, and prognostic value of cytotoxic T lymphocytes in follicular lymphoma: a 3-D tissue-imaging study. Blood. 2011;118(20):5371-5379.
13. Sugimoto T, Watanabe T. Follicular Lymphoma: The Role of the Tumor Microenvironment in Prognosis. J Clin Exp Hematop. 2016;56(1):1-19.
14. Glas AM, Knoops L, Delahaye L, et al. Gene-expression and immunohistochemical study of specific T-cell subsets and accessory cell types in the transformation and prognosis of follicular lymphoma. J Clin Oncol. 2007;25(4):390-398.
15. Radtke A, Postovalova E, Varlamova A, et al. A Multi-scale, Multiomic Atlas of Human Normal and Follicular Lymphoma Lymph Nodes. bioRxiv. 2022 June 5. https://doi.org/10.1101/2022.06.03.494716 [preprint, not peer-reviewed].

16. Han G, Deng Q, Marques-Piubelli ML, et al. Follicular Lymphoma Microenvironment Characteristics Associated with Tumor Cell Mutations and MHC Class II Expression. Blood Cancer Discov. 2022;3(5):428-443.
17. Laurent C, Dietrich S, Tarte K. Cell crosstalk within lymphoma tumor microenvironment: follicular lymphoma as a paradigm. Blood. 2024;143(12):1080-1090.
18. Amé-Thomas P, Tarte K. The yin and the yang of follicular lymphoma cell niches: Role of microenvironment heterogeneity and plasticity. Semin Cancer Biol. 2014;24:23-32.
19. Haebe S, Shree T, Sathe A, et al. Single-cell analysis can define distinct evolution of tumor sites in follicular lymphoma. Blood. 2021;137(21):2869-2880.
20. Grant SM, Lou M, Yao L, Germain RN, Radtke AJ. The lymph node at a glance - how spatial organization optimizes the immune response. J Cell Sci. 2020;133(5):jcs241828.
21. Hahne F, Khodabakhshi AH, Bashashati A, et al. Per-channel basis normalization methods for flow cytometry data. Cytometry A. 2010;77(2):121-131.
22. McInnes L, Healy J, Melville J. Umap: Uniform manifold approximation and projection for dimension reduction. arXiv. 2020 Sep 18. https://doi.org/10.48550/arXiv.1802.03426 [preprint, not peer-reviewed].
23. Van Gassen S, Callebaut B, Van Helden MJ, Lambrecht BN, Demeester P, Dhaene T, Saeys Y. FlowSOM: Using self-organizing maps for visualization and interpretation of cytometry data. Cytometry A. 2015;87(7):636-645.
24. Maecker HT, McCoy JP, Nussenblatt R. Standardizing immunophenotyping for the Human Immunology Project. Nat Rev Immunol. 2012;12(3):191-200.
25. Sage PT, Sharpe AH. T follicular regulatory cells in the regulation of B cell responses. Trends Immunol. 2015;36(7):410-418.
26. Sobhani N, Tardiel-Cyril DR, Davtyan A, Generali D, Roudi R, Li Y. CTLA-4 in Regulatory T Cells for Cancer Immunotherapy. Cancers (Basel). 2021;13(6):1440.
27. Banerjee H, Nieves-Rosado H, Kulkarni A, et al. Expression of Tim-3 drives phenotypic and functional changes in Treg cells in secondary lymphoid organs and the tumor microenvironment. Cell Rep. Sep 14 2021;36(11):109699.
28. Liu Z, McMichael EL, Shayan G, et al. Novel Effector Phenotype of Tim-3+ Regulatory T Cells Leads to Enhanced Suppressive Function in Head and Neck Cancer Patients. Clin Cancer Res. 2018;24(18):4529-4538.
29. Spasevska I, Sharma A, Steen CB, et al. Diversity of intratumoral regulatory T cells in B-cell non-Hodgkin lymphoma. Blood Adv. 2023;7(23):7216-7230.
30. Mulder TA, Wahlin BE, Österborg A, Palma M. Targeting the Immune Microenvironment in Lymphomas of B-Cell Origin: From Biology to Clinical Application. Cancers (Basel). 2019;11(7):915.
31. Kim JH, Kim BS, Lee SK. Regulatory T Cells in Tumor Microenvironment and Approach for Anticancer Immunotherapy. Immune Netw. 2020;20(1):e4.
32. Armengol M, Santos JC, Fernández-Serrano M, Profitós-Pelejà N, Ribeiro ML, Roué G. Immune-Checkpoint Inhibitors in B-Cell Lymphoma. Cancers (Basel). 2021;13(2):214.
33. Jacobson CA, Chavez JC, Sehgal AR, et al. Axicabtagene ciloleucel in relapsed or refractory indolent non-Hodgkin lymphoma (ZUMA-5): a single-arm, multicentre, phase 2 trial. Lancet Oncol. 2022;23(1):91-103.
34. Fowler NH, Dickinson M, Dreyling M, et al. Tisagenlecleucel in adult relapsed or refractory follicular lymphoma: the phase 2 ELARA trial. Nat Med. 2022;28(2):325-332.

35. Budde LE, Assouline S, Sehn LH, et al. Single-Agent Mosunetuzumab Shows Durable Complete Responses in Patients With Relapsed or Refractory B-Cell Lymphomas: Phase I Dose-Escalation Study. J Clin Oncol. 2022;40(5):481-491.
36. Yang ZZ, Kim HJ, Villasboas JC, et al. Mass Cytometry Analysis Reveals that Specific Intratumoral CD4(+) T Cell Subsets Correlate with Patient Survival in Follicular Lymphoma. Cell Rep. 2019;26(8):2178-2193.e3.
37. Mondello P, Fama A, Larson MC, et al. Lack of intrafollicular memory CD4□+□T cells is predictive of early clinical failure in newly diagnosed follicular lymphoma. Blood Cancer J. 2021;11(7):130.
38. Okeke EB, Uzonna JE. The Pivotal Role of Regulatory T Cells in the Regulation of Innate Immune Cells. Front Immunol. 2019;10:680.
39. Yang ZZ, Novak AJ, Stenson MJ, Witzig TE, Ansell SM. Intratumoral CD4+CD25+ regulatory T-cell-mediated suppression of infiltrating CD4+ T cells in B-cell non-Hodgkin lymphoma. Blood. 2006;107(9):3639-3646.
40. Joller N, Lozano E, Burkett PR, et al. Treg cells expressing the coinhibitory molecule TIGIT selectively inhibit proinflammatory Th1 and Th17 cell responses. Immunity. 2014;40(4):569-581.
41. Sakuishi K, Ngiow SF, Sullivan JM, Teng MW, Kuchroo VK, Smyth MJ, Anderson AC. TIM3(+)FOXP3(+) regulatory T cells are tissue-specific promoters of T-cell dysfunction in cancer. Oncoimmunology. 2013;2(4):e23849.
42. Fazilleau N, Aloulou M. Several Follicular Regulatory T Cell Subsets With Distinct Phenotype and Function Emerge During Germinal Center Reactions. Front Immunol. 2018;9:1792.
43. Hao H, Nakayamada S, Tanaka Y. Differentiation, functions, and roles of T follicular regulatory cells in autoimmune diseases. Inflamm Regen. 2021;41(1):14.
44. Wing JB, Kitagawa Y, Locci M, et al. A distinct subpopulation of CD25(-) T-follicular regulatory cells localizes in the germinal centers. Proc Natl Acad Sci U S A. 2017;114(31):E6400-E6409.
45. Yang ZZ, Grote DM, Xiu B, et al. TGF-β upregulates CD70 expression and induces exhaustion of effector memory T cells in B-cell non-Hodgkin's lymphoma. Leukemia. 2014;28(9):1872-1884.
46. Shibamiya A, Miyamoto-Nagai Y, Koide S, et al. The pathogenetic significance of exhausted T cells in a mouse model of mature B cell neoplasms. Cancer Immunol Immunother. 2023;72(8):2635-2648.
47. Yang ZZ, Grote DM, Ziesmer SC, Xiu B, Novak AJ, Ansell SM. PD-1 expression defines two distinct T-cell sub-populations in follicular lymphoma that differentially impact patient survival. Blood Cancer J. 2015;5(2):e281.

Table 1. Patient clinicopathologic characteristics

Characteristics at time of biopsy	Follicular Hyperplasia	Follicular Lymphoma	
		Untreated	Relapsed/Refractory
Number of Cases	43	54	37
Age at biopsy, median years (range)	56 (12-86)	65 (33-89)	56 (37-79)
Gender (F/M)	31/12	32/22	14/23
Anatomic site			
Nodal, n (%)	43 (100)	53 (98)	32 (86)
Axillary	19	6	5
Cervical	13	14	3
Head	0	3	3
Inguinal	2	16	10
Retroperitoneal	1	7	3
Thoracic	4	0	2
Tonsil	2	1	1
Other	2	6	5
Spleen, n (%)	0 (0)	1 (2)	0 (0)
Extranodal, n (%)	0(0)	0 (0)	4 (11)
Diagnosis			
FL Grade 1-2, n (%)	-	43 (80)	31 (84)
FL Grade 3A, n (%)	-	9 (17)	5 (14)
FL Grade 3B, n (%)	-	2 (4)	1 (3)
Stage at biopsy			
1-2, n (%)	-	8 (17)	2 (6)
3-4, n (%)	-	40 (83)	33 (94)
FLIPI at sampling, median (range)		2 (0-5)	2 (0-5)
0-1, n (%)	-	10 (21)	10 (29)
2, n (%)	-	20 (42)	13 (37)
3-5, n (%)	-	18 (38)	12 (34)
History of aggressive lymphoma prior to biopsy	-	0	9
Prior lines of therapy, median (range)		0 (0)	1 (1-6)
1	-	-	8
2	-	-	1
3	-	-	0
4	-	-	2

>4	-	-	3
POD24 after initial therapy, n (%)	-	-	17 (49)
Prior anti-CD20, n (%)	-	-	34 (97)
Prior Chemotherapy, n (%)	-	-	28 (80)
Anthracycline-containing, n (%)	-	-	21 (60)
Bendamustine-containing, n (%)	-	-	10 (29)
Post-Biopsy Outcomes	**Follicular Hyperplasia**	**Follicular Lymphoma**	
		Untreated (N=48)	**Relapsed/Refractory (N=35)**
Treated after biopsy, n (%)	-	36 (75)	34 (97)
Median time to treatment (range in days)	-	32 (6-591)	30 (9 - 556)
Treated within 6 months of sample, n (%)	-	29 (60)	30 (86)
Treated more than 6 months after sample, n (%)	-	7 (15)	4 (11)
Treatment Regimen	-		
Radiation only, n (%)	-	6 (17)	5 (15)
Rituximab monotherapy, n (%)	-	5 (14)	6 (18)
R- or O-Chemo, n (%)	-	24 (67)	9 (26)
Bendamustine, n (%)	-	8 (22)	5 (15)
CHOP, n (%)	-	15 (42)	3 (9)
Other, n (%)	-	1 (3)	1 (3)
R- or O-lenalidomide, n (%)	-	1 (3)	8 (24)
Other, n (%)	-	0 (0)	6 (18)
POD after treatment, n (%)	-	13 (36)	20 (59)
Progression within 24 months (POD24), n (%)	-	10 (28)	16 (47)
Median Follow-up, years (range)		3.1 (0.5 - 3.7)	3.1 (0.4 - 3.9)
Transformation during follow-up, n (%)	-	4 (8.3)	3 (8.6)
Death during follow-up, n (%)		4 (8.3)	5 (14)

Abbreviations: FL, follicular lymphoma; FLIPI, Follicular lymphoma international prognostic index; POD24, progression of disease within 24 months of initial treatment; R-, rituximab; O-, obinutuzumab

Table 2. T-cell repertoire of the follicular hyperplasia and follicular lymphoma cohorts

Population name			Immunophenotype	Median (count/1000)			Adjusted pairwise p-value		
				FH	FL-UT	FL-RR	FH vs FL-UT	FH vs FL-RR	FL-UT vs FL-RR
CD4+	Naïve		CD45RO-, CCR7+	296.445	165.89	78.352	0.001 ↓	0.001 ↓	ns
	Memory	CM	CD45RO+, CCR7+, CD95+	200.922	127.411	128.259	0.002 ↓	0.003 ↓	ns
		EM PT	CD45RO+, CCR7-, CD95+, TIGITdim, PD1dim	39.289	47.593	41.832	ns	ns	ns
		EM PTC	CD45RO+, CCR7-, CD95+, TIGIT+, PD1+, CTLA4+	25.973	39.788	34.659	ns	ns	ns
		EM PTCTi	CD45RO+, CCR7-, CD95+, TIGIT+, PD1+, CTLA4+, TIM3+	5.368	10.676	9.146	0.001 ↑	0.002 ↑	ns
	TFH		CD45RO+, CCR7-, CD95+, CTLA4+, TIGIT+, PD1bright	59.724	148.957	137.775	0.001 ↑	0.002 ↑	ns
	TFR		FoxP3+, CD25dim/-, CD45RO+, CCR7-, CD95+, CTLA4+, TIGIT+, PD1+, CXCR5+	10.605	32.946	48.33	0.001 ↑	0.001 ↑	0.018 ↑
	TFR-like		FoxP3+, CD25-, CD45RO+, CCR7-, CD95+, CTLA4dim, TIGITdim, PD1-	12.812	15.505	15.195	ns	ns	ns
	Effector		CD45RO-, CCR7-, CD95dim, CD96+, TIM3+	13.389	4.691	3.536	0.001 ↓	0.001 ↓	ns
	T-Reg	Naïve	FoxP3+, CD25, CD45RO-, CCR7-, CD95-	8.755	6.156	4.95	ns	0.001 ↓	0.04 ↓
		EM	FoxP3+, CD25dim, CD45ROdim, CCR7-, CD95dim, CTLA4dim, TIGITdim	44.577	40.958	35.595	ns	ns	ns
		TC	FoxP3+, CD25+, CD45RO+, CCR7-, CD95+, CTLA4+, TIGIT+,PD1dim	21.584	48.132	51.255	0.001 ↑	0.001 ↑	ns
		PTCTi	FoxP3+, CD25+, CD45RO+, CCR7-, CD95+, CTLA4+, TIGIT+, PD1+, TIM3+	5.018	22.977	30.144	0.001 ↑	0.001 ↑	ns
CD8+	Naïve		CD45RO-, CCR7+, CD73+	63.242	24.299	31.259	0.001 ↓	ns	ns
	Memory	CM/EM	CD45RO+, CCR7dim+/-, CD95+, CD73dim	21.53	14.263	17.02	ns	ns	ns
		EM PT	CD45RO+, CCR7-, CD95+, CD96, TIGITdim, PD1dim	21.095	43.211	52.553	0.001 ↑	0.001 ↑	ns
		EM PTC	CD45RO+, CCR7-, CD95+, CTLA4+, TIGIT+, PD1+, Ki67±	1.06	6.924	10.375	0.001 ↑	0.001 ↑	ns

		EM PTCTi	CD45RO+, CCR7-, CD95+, TIGIT+, PD1+, TIM3+, CTLA4+	3.456	30.669	37.726	0.001 ↑	0.001 ↑	ns
	Effector		CD45RO-, CCR7-, CD95+, TIGITdim, Tbet dim	8.339	10.397	12.209	ns	ns	ns

Abbreviations: CM, central memory; EM, effector memory; FH, Follicular hyperplasia; FL-RR, Follicular lymphoma relapsed/refractory; FL-UT, Follicular lymphoma untreated; TFH, T-follicular helper cells; TFR, T-follicular regulatory cells; PT, PD1+TIGIT+; PTC, PD1+TIGIT+CTLA-4+; PTCTi, PD1+TIGIT+CTAL-4+TIM3+, TC, TIGIT+CTLA-4+; ns, not significant

Figure legends

FIGURE 1: Distribution and immunophenotyping of CD3+ T-cells in reactive follicular hyperplasia (FH), untreated follicular lymphoma (FL-UT) and relapsed/refractory follicular lymphoma (FL-RR) lymph node specimens. Using the pipeline illustrated in Figure S1, 13 CD4+ and 6 CD8+ T-cell subsets were identified. **(A)** Distribution of CD4+ and CD8+ T-cell subsets in FH, FL-UT and FL-RR. **(B)** Uniform Manifold Approximation and Projection (UMAP) of CD4+ and CD8+ T-cell subsets in FH, FL-UT and FL-RR. **(C)** Heatmap generated using the mean surface marker expression in each cluster.

FIGURE 2: Distribution of T-regulatory cells (naïve and highly suppressive), T-follicular helper cells (TFH) and T-follicular regulatory cells (TFR) in FH, FL-UT and FL-RR. **(A)** Histograms showing percentage of T-reg, TFH and TFR subsets in the CD3+ compartment. **(B)** UMAP of T-regs, TFH and TFR. **(C)** Phenotype comparison between the T-reg sub-populations, TFR, TFH and the total CD3+ T-cell population. **(D)** Additional characterization of total T-regulatory cells, TFR and TFH using research panel II and the gate strategy indicated in Figure S5. p- value *** ≤ 0.001 ** ≤ 0.002 *≤ 0.05

FIGURE 3: Distribution of CD3+ subpopulations expressing inhibitory immune checkpoint receptors in CD4 and CD8 compartments. (A-B) Distribution of effector memory CD4+ and CD8+ subpopulations expressing the inhibitory immune checkpoint receptors PD1 and TIGIT (EM PT); PD1, TIGIT and CTLA-4 (EM PTC); PD1, TIGIT, CTLA-4 and TIM3 (EM PTCTi). **(C-D)** UMAP of various inhibitory immune checkpoint receptors expressing CD4+ and CD8+ subpopulations (on the left) and their phenotype comparison (on the right). p- value *** ≤ 0.001 ** ≤ 0.002

FIGURE 4: Multiplex immunofluorescence (MxIF) assay using antibodies against CD4, PD1, FoxP3 and BCL6 and its comparison to flow cytometric evaluation on FH, FL-UT and FL-RR specimens. (A) MxIF images demonstrating CD4+ PD (dim)+ FoxP3+ TFR cells and CD4+ BCL6+ PD1+ TFH cells on FH, FL-UT and FL-RR specimens. **(B)** Linear regression analysis for TFR and TFH subpopulations as evaluated by MxIF vs. flow cytometry.

FIGURE 5: Correlation of T-reg TC and TFH with earlier initiation of the therapy in FL-UT cohort. (A-B) T-reg TC and TFH represented as percent of WBC plotted against time to first treatment (≤3 months, n=28; >3 months, n=8; treatment naïve, n=12). **(C)** Kaplan Meier curve illustrating time to first treatment of the 2 cohorts based on optimal cutoff threshold for T-reg TC percentage. **(D)** Kaplan Meier curve illustrating time to first treatment of the 2 cohorts based on optimal cutoff threshold for TFH percentage.

FIGURE 6: Unsupervised hierarchical clustering of T-cells subsets as a percentage of WBC showing FL cases clustering together in clusters #1 and #2 while FH cases being enriched in cluster #3.

Figure 1

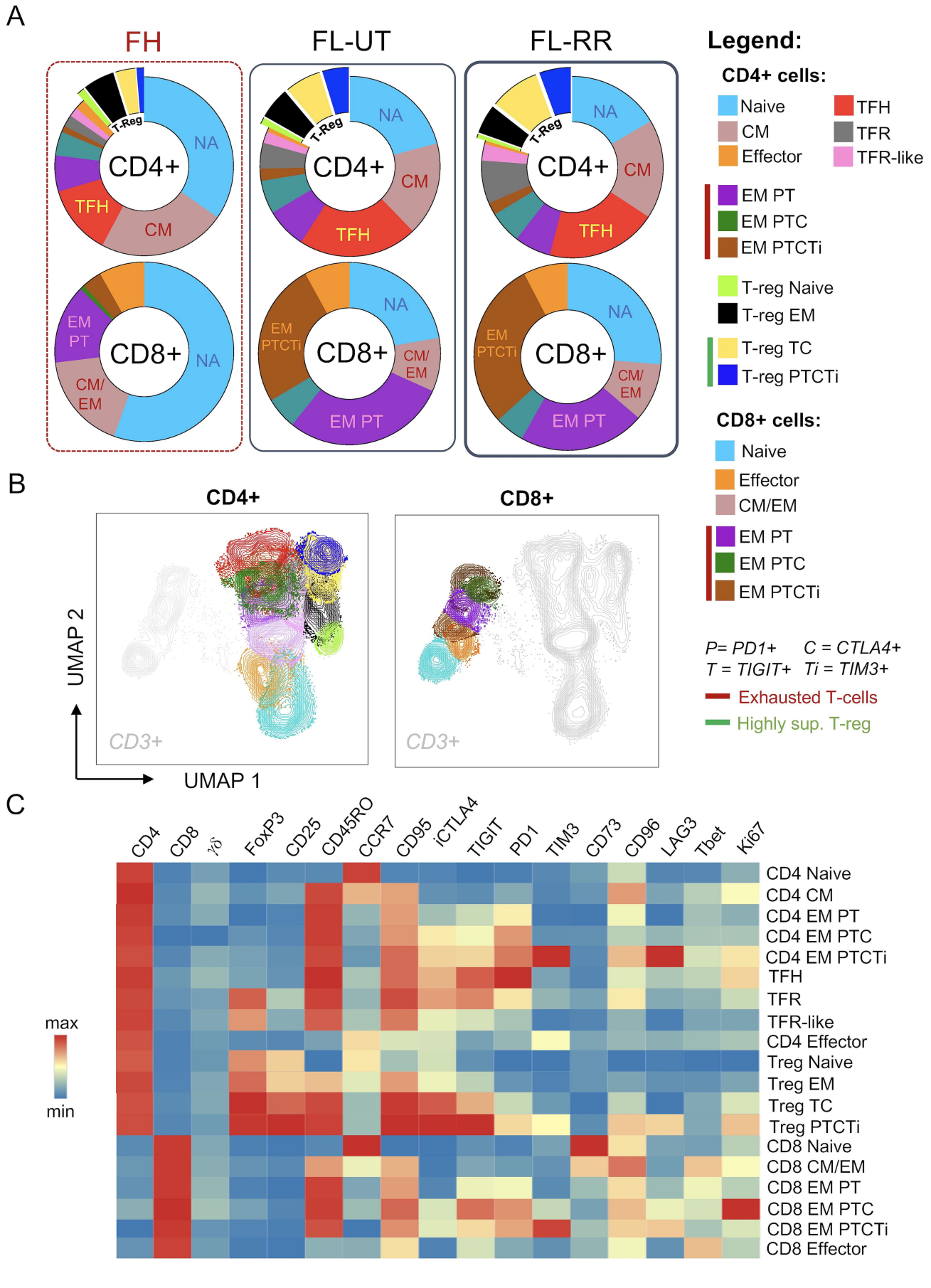
A
FH
FL-UT
FL-RR
CD4+
CD8+
T-Reg
NA
CM
TFH
EM PT
EM PTCTi
CM/ EM
Legend:
CD4+ cells:
Naive
TFH
CM
TFR
Effector
TFR-like
EM PT
EM PTC
EM PTCTi
T-reg Naive
T-reg EM
T-reg TC
T-reg PTCTi
CD8+ cells:
Naive
Effector
CM/EM
EM PT
EM PTC
EM PTCTi
P= PD1+ C = CTLA4+
T = TIGIT+ Ti = TIM3+
Exhausted T-cells
Highly sup. T-reg
B
CD4+
CD8+
UMAP 2
UMAP 1
CD3+
C
CD4
CD8
γδ
FoxP3
CD25
CD45RO
CCR7
CD95
iCTLA4
TIGIT
PD1
TIM3
CD73
CD96
LAG3
Tbet
Ki67
max
min
CD4 Naive
CD4 CM
CD4 EM PT
CD4 EM PTC
CD4 EM PTCTi
TFH
TFR
TFR-like
CD4 Effector
Treg Naive
Treg EM
Treg TC
Treg PTCTi
CD8 Naive
CD8 CM/EM
CD8 EM PT
CD8 EM PTC
CD8 EM PTCTi
CD8 Effector

Figure 2

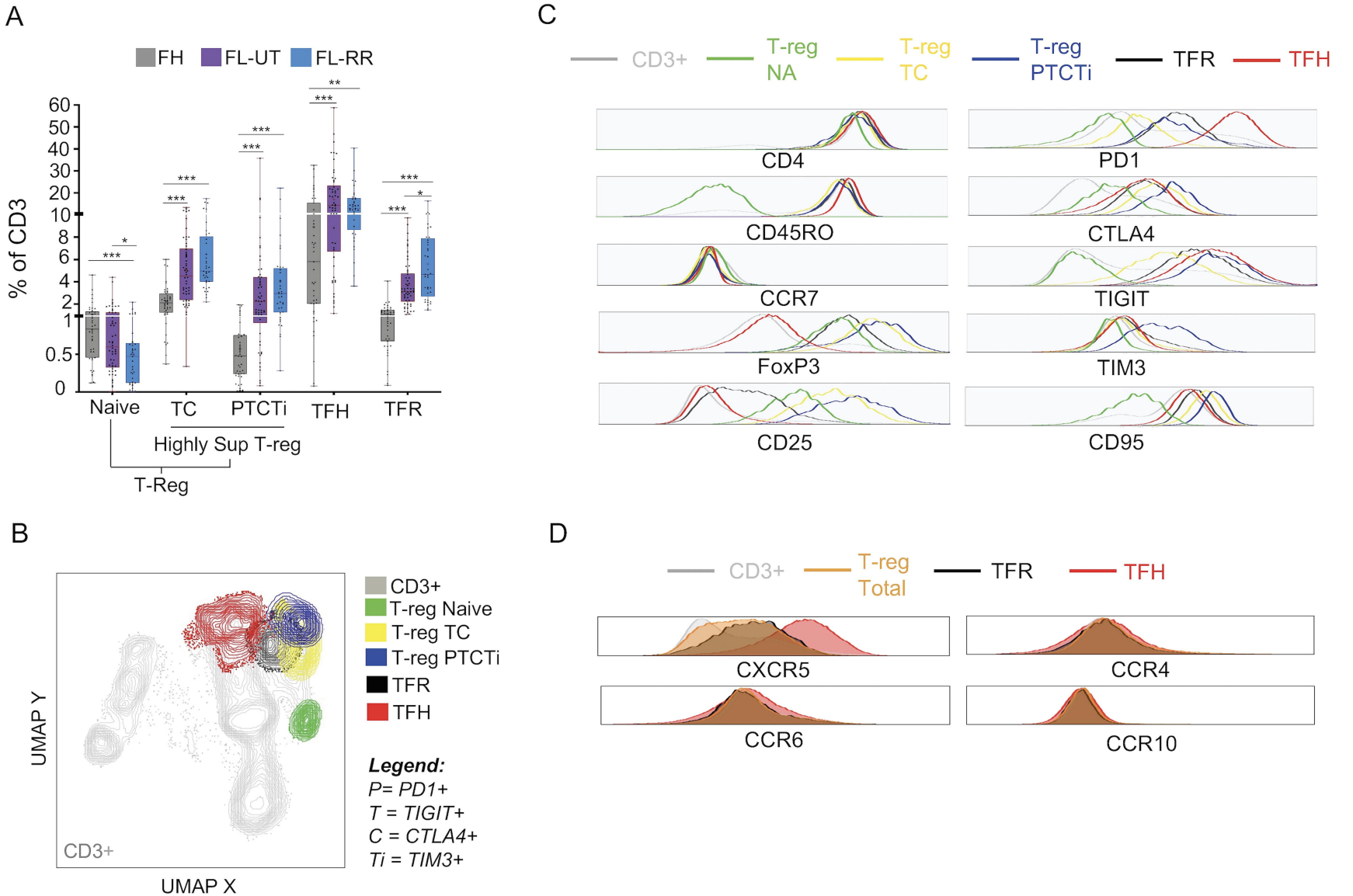
A
FH
FL-UT
FL-RR
% of CD3
Naive
TC
PTCTi
TFH
TFR
Highly Sup T-reg
T-Reg
B
CD3+
T-reg Naive
T-reg TC
T-reg PTCTi
TFR
TFH
Legend:
P= PD1+
T = TIGIT+
C = CTLA4+
Ti = TIM3+
UMAP Y
UMAP X
C
CD3+
T-reg NA
T-reg TC
T-reg PTCTi
TFR
TFH
CD4
PD1
CD45RO
CTLA4
CCR7
TIGIT
FoxP3
TIM3
CD25
CD95
D
CD3+
T-reg Total
TFR
TFH
CXCR5
CCR4
CCR6
CCR10

Figure 3

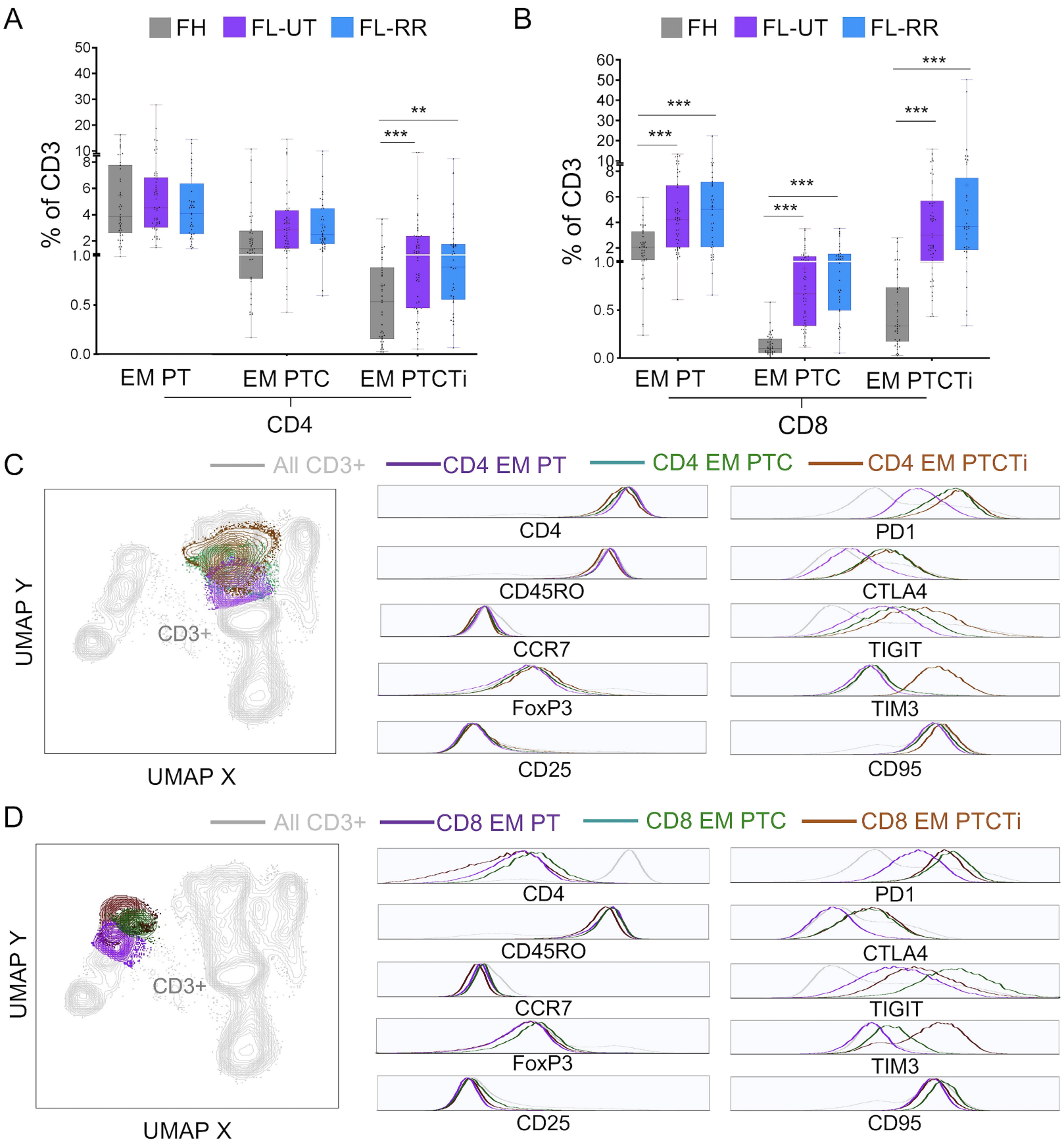
A
FH
FL-UT
FL-RR
% of CD3
EM PT
EM PTC
EM PTCTi
CD4
B
FH
FL-UT
FL-RR
% of CD3
EM PT
EM PTC
EM PTCTi
CD8
C
All CD3+
CD4 EM PT
CD4 EM PTC
CD4 EM PTCTi
UMAP Y
CD3+
UMAP X
CD4
PD1
CD45RO
CTLA4
CCR7
TIGIT
FoxP3
TIM3
CD25
CD95
D
All CD3+
CD8 EM PT
CD8 EM PTC
CD8 EM PTCTi
UMAP Y
CD3+
UMAP X
CD4
PD1
CD45RO
CTLA4
CCR7
TIGIT
FoxP3
TIM3
CD25
CD95

Figure 4

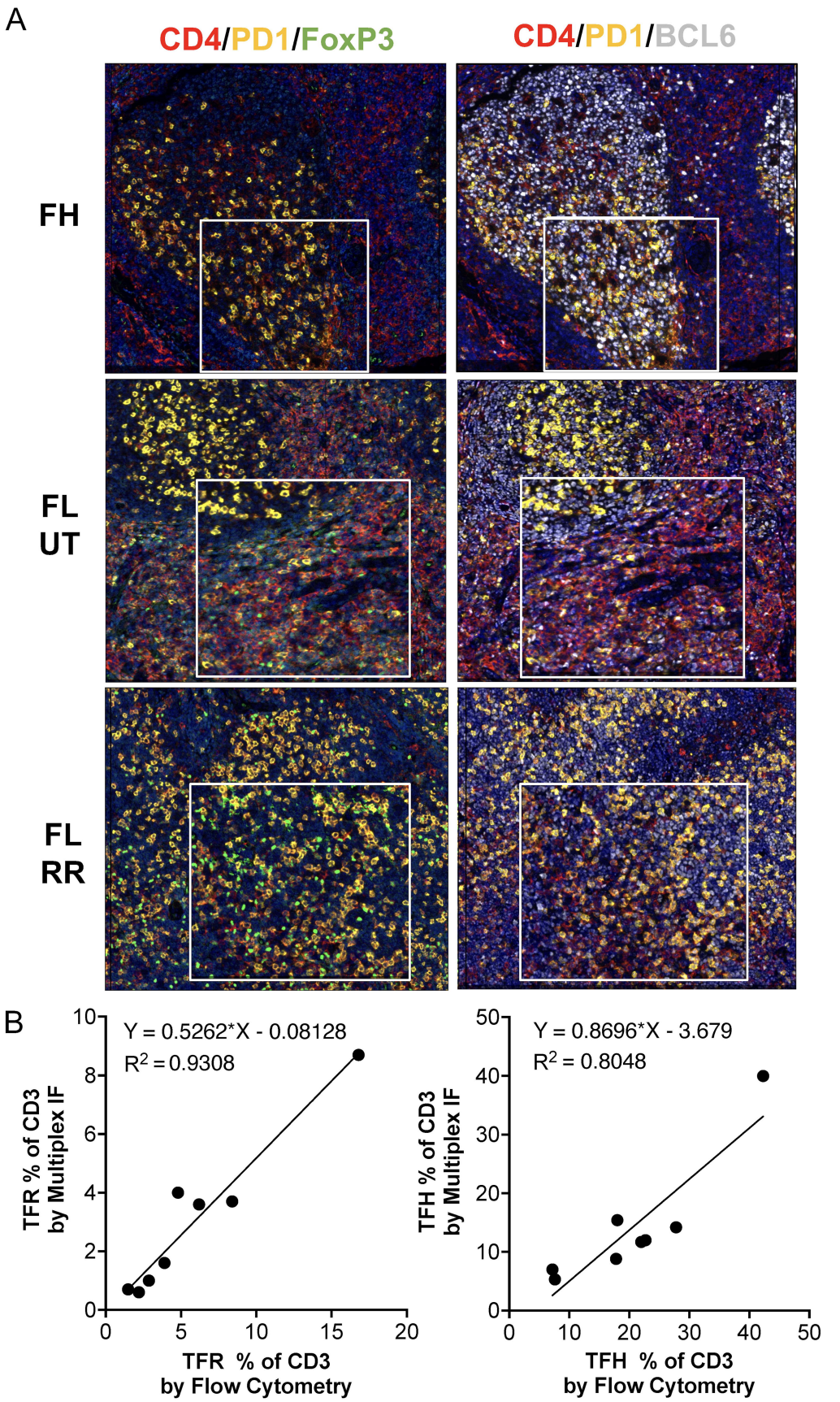
A
CD4/PD1/FoxP3
CD4/PD1/BCL6
FH
FL UT
FL RR
B
Y = 0.5262*X - 0.08128
R2 = 0.9308
TFR % of CD3 by Multiplex IF
TFR % of CD3 by Flow Cytometry
Y = 0.8696*X - 3.679
R2 = 0.8048
TFH % of CD3 by Multiplex IF
TFH % of CD3 by Flow Cytometry

Figure 5

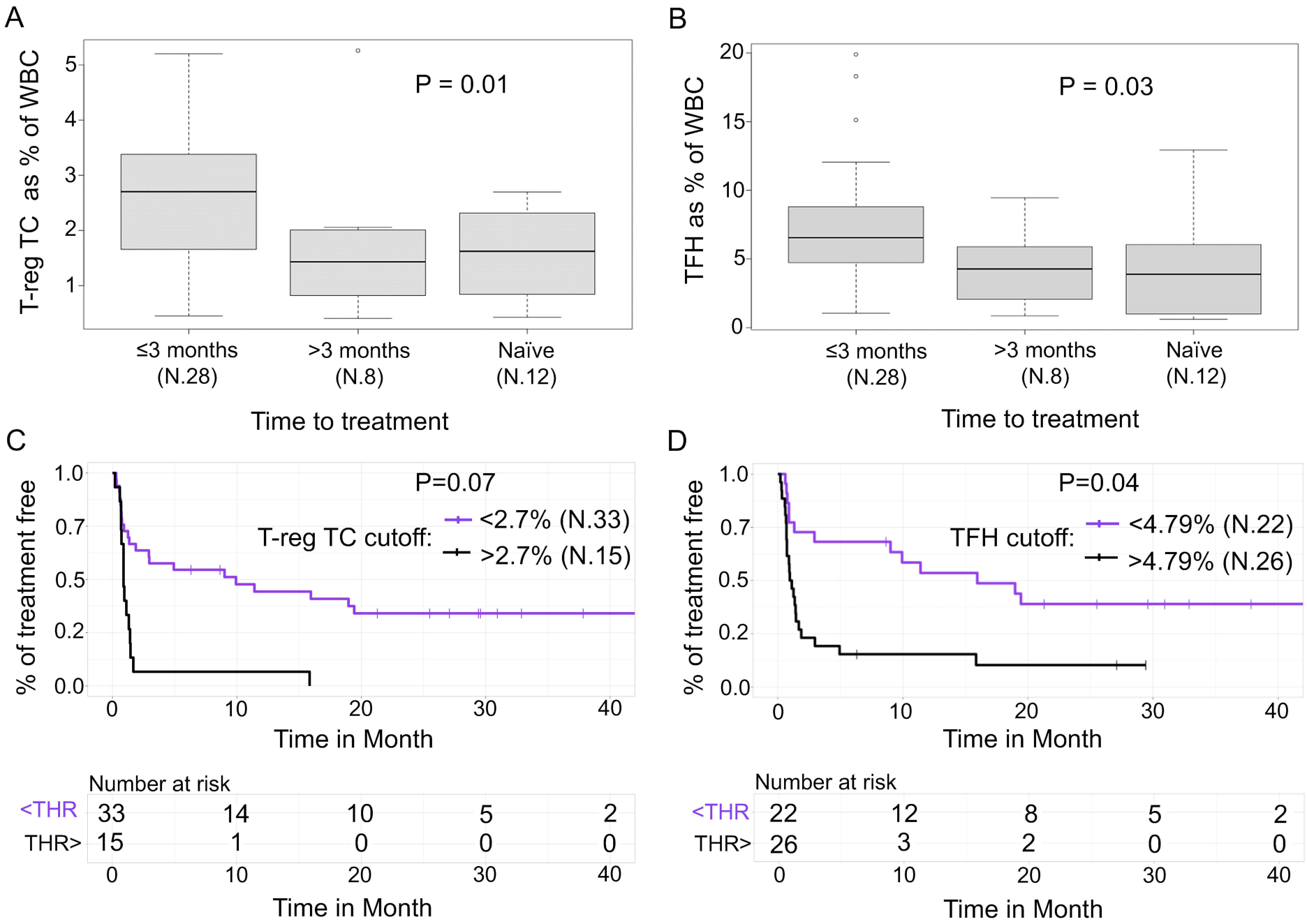
A
T-reg TC as % of WBC
P = 0.01
≤3 months (N.28)
>3 months (N.8)
Naïve (N.12)
Time to treatment
B
TFH as % of WBC
P = 0.03
≤3 months (N.28)
>3 months (N.8)
Naïve (N.12)
Time to treatment
C
% of treatment free
P=0.07
T-reg TC cutoff:
<2.7% (N.33)
>2.7% (N.15)
Time in Month
Number at risk
<THR 33 14 10 5 2
THR> 15 1 0 0 0
Time in Month
D
% of treatment free
P=0.04
TFH cutoff:
<4.79% (N.22)
>4.79% (N.26)
Time in Month
Number at risk
<THR 22 12 8 5 2
THR> 26 3 2 0 0
Time in Month

Figure 6

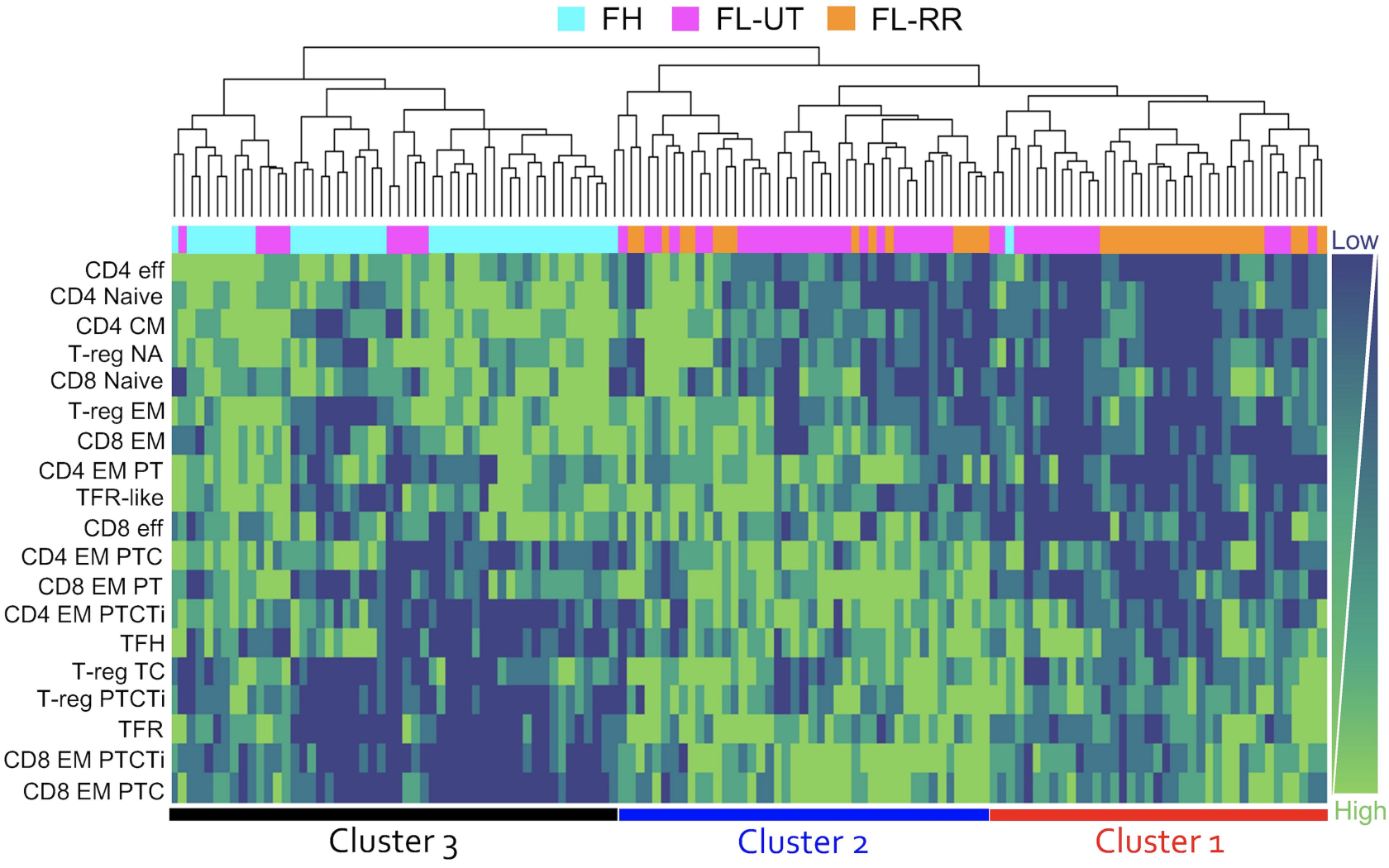
FH
FL-UT
FL-RR
Low
High
CD4 eff
CD4 Naive
CD4 CM
T-reg NA
CD8 Naive
T-reg EM
CD8 EM
CD4 EM PT
TFR-like
CD8 eff
CD4 EM PTC
CD8 EM PT
CD4 EM PTCTi
TFH
T-reg TC
T-reg PTCTi
TFR
CD8 EM PTCTi
CD8 EM PTC
Cluster 3
Cluster 2
Cluster 1

Deep immunophenotypic dissection and clinical impact of T-cells in the follicular lymphoma microenvironment

Running title: Follicular Lymphoma T-cell Microenvironment

Sary El Daker[1], David Qualls[2], Andriy Derkach[3], Samida Beqaj[1], Leonardo Boiocchi[1], Venkatraman Seshan[3], Jeeyeon Baik[1], Menglei Zhu[1], Gilles Salles[2], Ahmet Dogan[1], Mikhail Roshal[1], Pallavi Galera[1].

[1] Hematopathology Service, Department of Pathology and Laboratory Medicine*

[2] Lymphoma Service, Department of Medicine

[3] Department of Epidemiology and Biostatistics

* A member of the imCORE Network

Memorial Sloan Kettering Cancer Center, New York, NY, USA

Supplementary Methods

Cell processing/staining and acquisition

Flow cytometry staining was performed using standard protocols for nuclear markers provided by Invitrogen (FoxP3/Transcription factor staining buffer set). Tissue samples were placed into a 70mm cell strainer on top of a conical 50mL tube containing RPMI-1640, 10% NBCS and penicillin/streptomycin preparation. The thumb press of a 1mL syringe plunger was used to crush the sample and dissociate the cells. The strainer was washed periodically until all the tissue was dissociated. The strained cell suspension was washed twice, and cells were finally counted and resuspended at the designed concentration. Tissue suspensions were stained with a cocktail of surface antibodies for 15 minutes at room temperature. Cells were washed with PBA buffer, and the cell pellets were resuspended in Fix/Perm working solution. After 15 minutes of incubation at room temperature protected from light, cells were washed with Perm buffer 1X, and the pellet was resuspended in 200 microliters of a cocktail containing antibodies directed towards intracellular antigens (FoxP3, Tbet, Ki67, and CTLA4). Cells were incubated for 30 min at room temperature, protected from light. After incubation, cells were washed twice in Perm buffer and resuspended in 100 microliters of PBA.

Multiplex immunofluorescence

Tissue sections were prepared for a 6-plex immunofluorescence assay targeting CD20, CD4, FoxP3, PD-1 and BCL-6 antigens (Table S3). Staining was performed on the Leica BOND RX automatic staining platform. Antigen retrieval was performed using the Epitope Retrieval Solution 2, incubated for 20 mins on the BOND. The sections were then incubated sequentially with the primary antibodies each diluted to varying concentrations after validation on control tissue. Each antibody was followed by the secondary polymer SuperBoost™ Goat anti-Mouse Poly HRP or SuperBoost™ Goat anti-Rabbit Poly HRP (ThermoFisher) and its corresponding fluorophore from Akoya Bioscience's Opal 6-Plex Detection Kit. After staining is complete, the slides were counterstained with DAPI and then mounted with ProLong Gold antifade reagent (ThermoFisher). The slides were imaged using the Vectra Polaris PhenoImager (Akoya Bioscience), and then analyzed using the image analysis platform HALO.

Statistical analysis

The proportions of T-cell populations were tested across the cohorts using the Kruskal-Wallis test. Pairwise comparison was performed when the Kruskal-Wallis test was significant and a Bonferroni correction was applied. The cell counts obtained from the cell processing step for the 19 T-cell subsets were normalized to express the counts as number per 1000 cells to account for varying total cell counts across samples.

For the unsupervised clustering of the samples the normalized data were further categorized into quartiles of the distribution of normalized cell counts across samples. This categorization accounts for the difference in median cell counts by immune cell type as well as the skewness in the distributions. The cell counts across the three classes were compared using Kruskal-Wallis test. Closed testing procedure with Bonferroni correction was used for pairwise comparisons for immune cell types for which the null hypothesis of same distributions for all three groups was rejected.

Similarly, associations between clinical variables and percentages of immune suppressive populations were evaluated by using Kruskal-Wallis test. Selection cut-off thresholds for these continuous biomarkers for optimal association with time to start of a treatment was conducted using maximally selected rank statistics.[1] Lastly associations between clusters and time to event outcomes were evaluated by log-rank test.

Supplementary Figure 1:

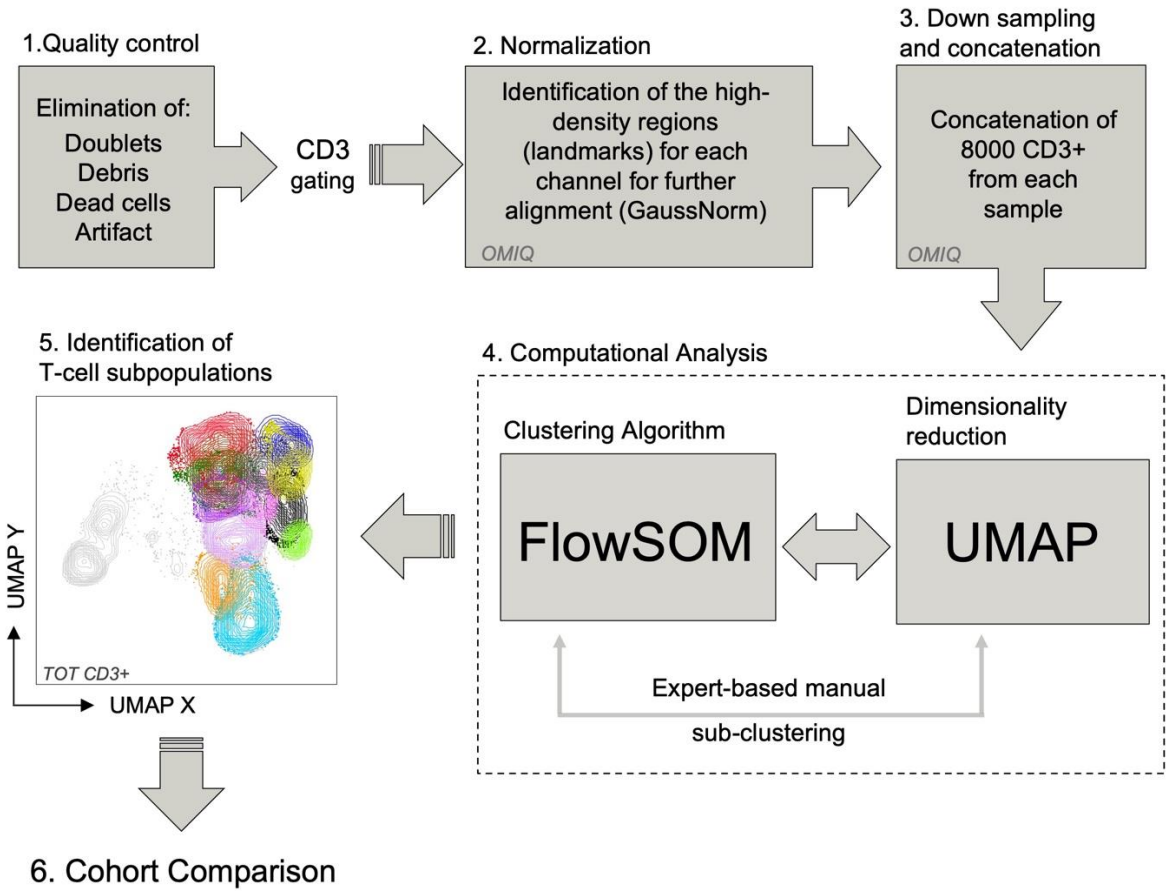

Figure S1. Overview of the analytical pipeline used to analyze single-cell suspensions derived from reactive and B-cell lymphoma isolates. Research Panel I was been analyzed using the following pipeline: scatter parameters were used to remove doublets, debris, dead cells and artifacts from every single file. T cells were identified using CD3 antibody and scatter parameters and used as input for the analytical pipeline. To minimize technical variation in sample acquisition over time we used an R-based algorithm (GaussNorm). 8000 CD3+ events from each sample were concatenated and the file generated (containing both reactive follicular hyperplasia and follicular lymphoma specimens) was used to identify the T-cell subpopulations by combining a dimensionality reduction technique (UMAP) with an unsupervised clustering algorithm (FlowSOM). Expert-based manual sub-clustering was performed to refine phenotypes that showed excessive heterogeneity.

Supplementary Figure 2:

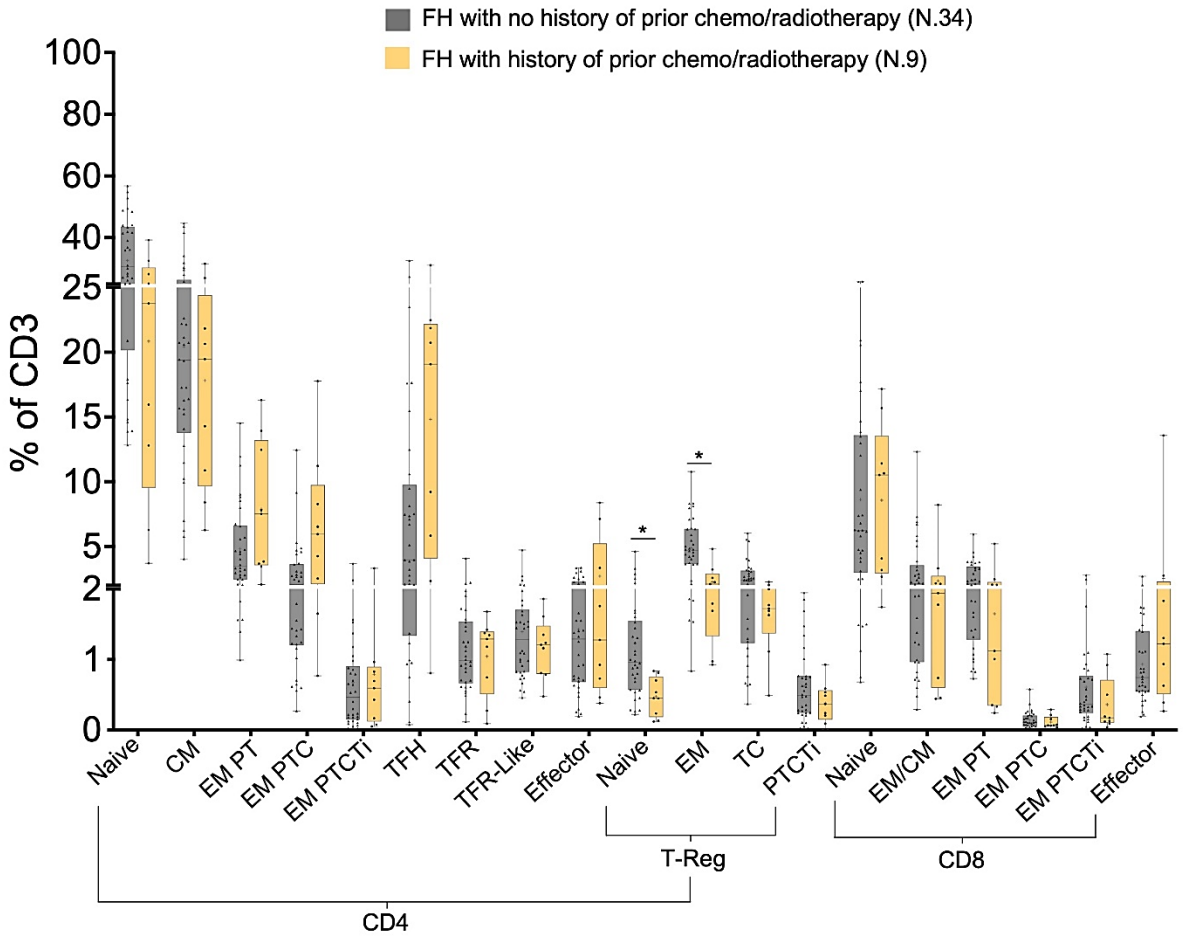

Figure S2. Distribution of various T-cell subsets in FH cohort comparing patients with no history of prior chemo/radiotherapy and patients with prior therapy.

Supplementary Figure 3:

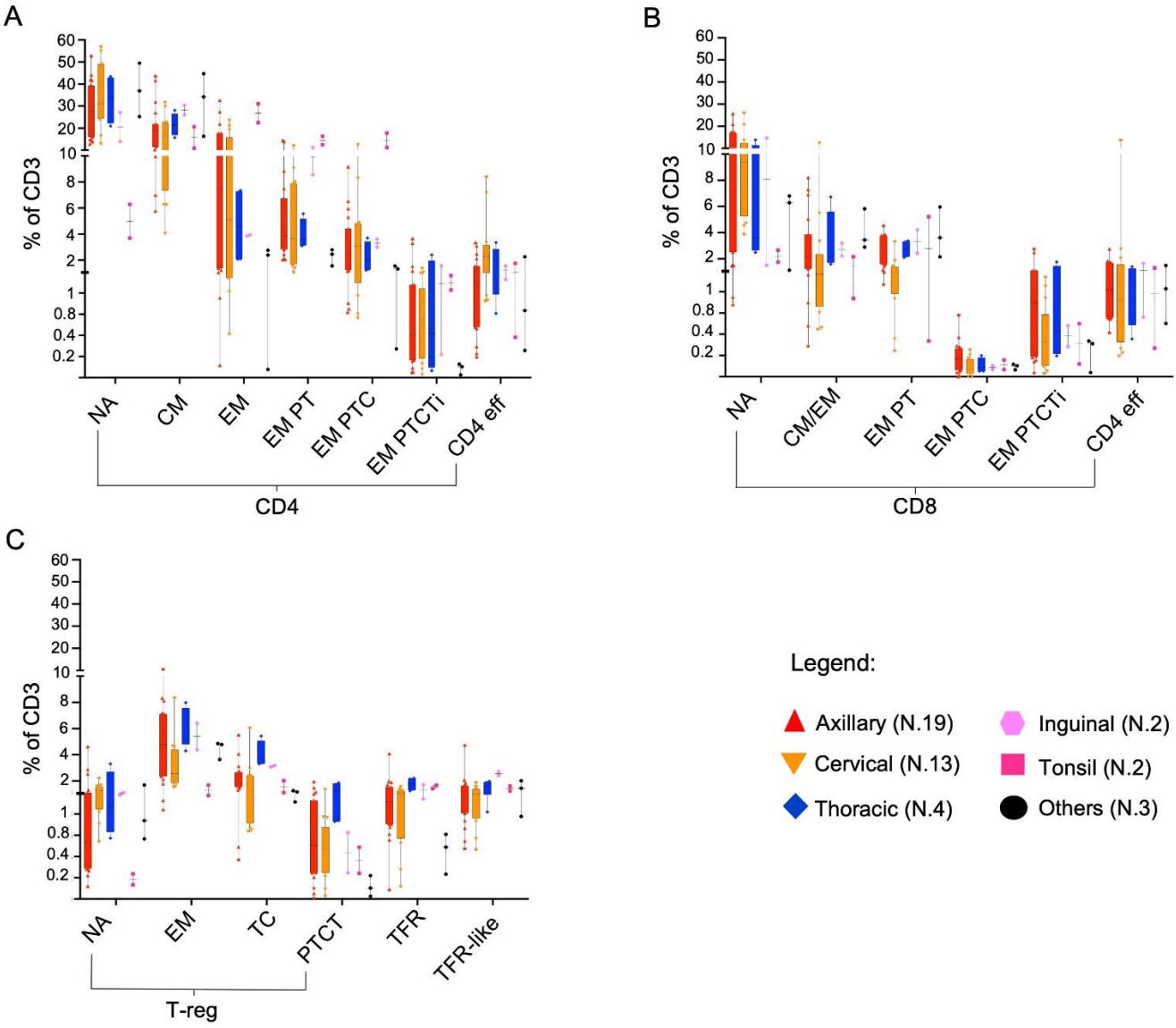

Figure S3. Distribution of various T-cell subsets in FH cohort comparing various anatomical sites of sampling.
(A) CD4+ T-cell subsets. (B) CD8+ T-cell subsets. (C) T-regulatory cells.

Supplementary Figure 4:

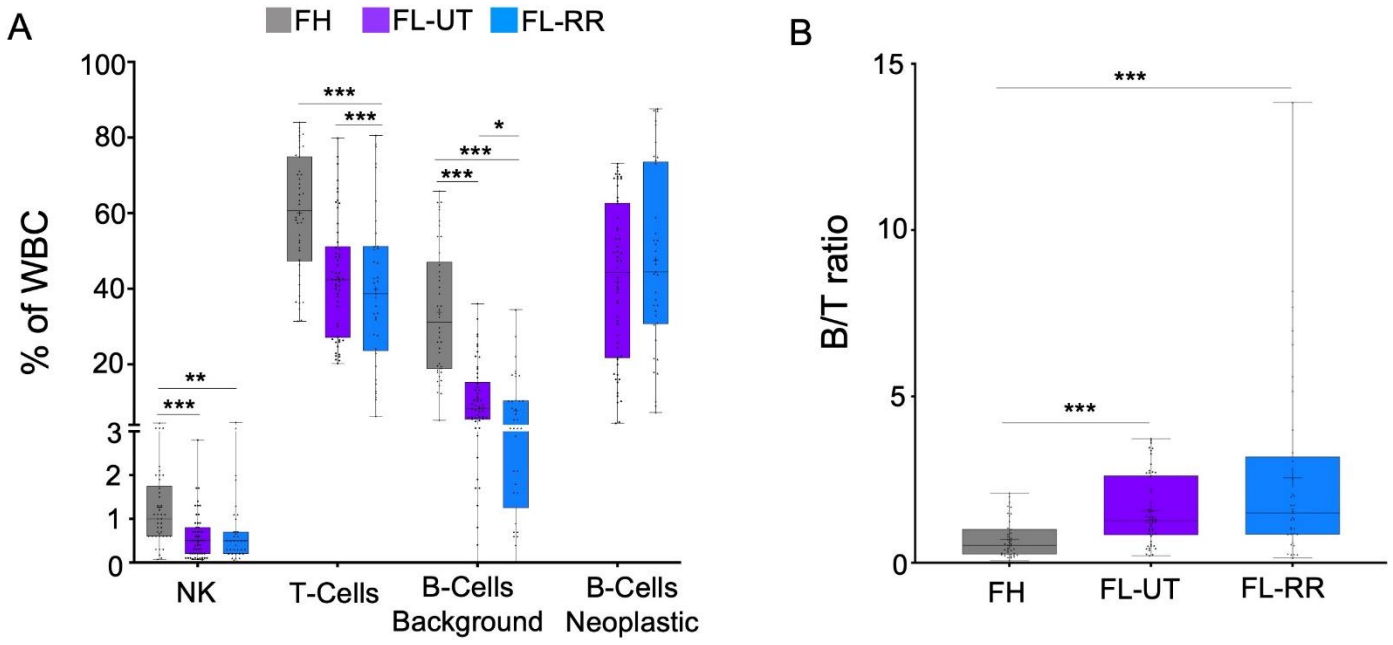

Figure S4. Clinical characterization of reactive (FH) and follicular lymphoma (FL-UT, FL-RR) specimens. (A) Percentage of NK-cells, T-cells, background non-neoplastic B-cells and neoplastic B-cells in FH and FL specimens (FL-UT and FL-RR). (B) B/T ratio in FH and FL specimens. p- value *** ≤ 0.0001 ** ≤ 0.001 *≤ 0.02

Supplementary Figure 5:

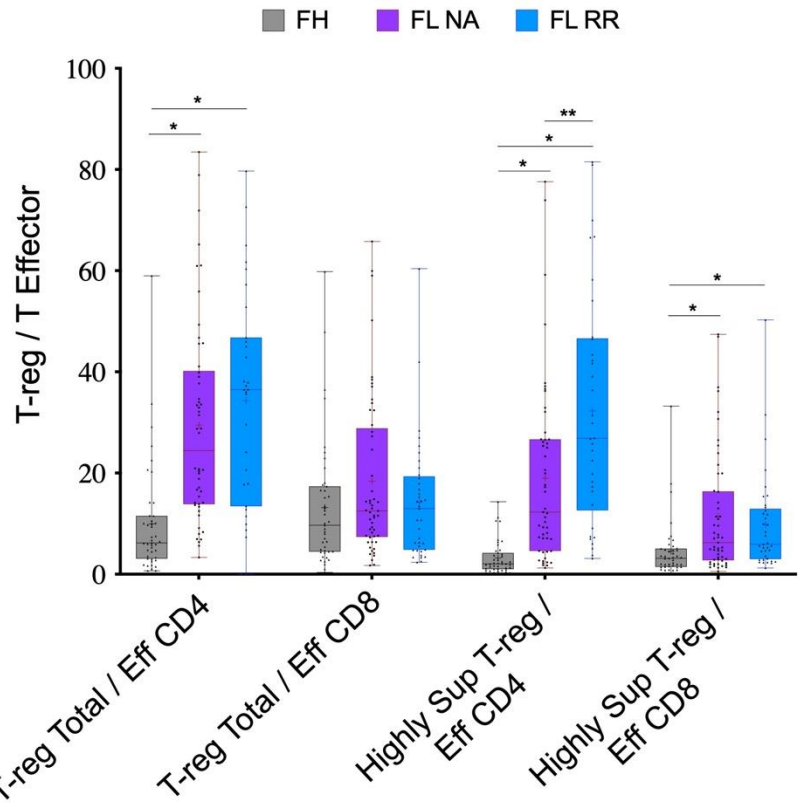

Figure S5. Regulatory T-reg/Effector T cells ratio in reactive (FH) and follicular lymphoma (FL-UT, FL-RR) specimens. Ratio between T-reg Total (T-reg naïve, T-reg EM, T-reg TC and Treg PTCTi), Highly suppressive T-reg (T-reg TC and T-reg PTCTi) and effector CD4 and effector CD8 was calculated. p- value ** ≤ 0.001 *≤ 0.02

Supplementary Figure 6:

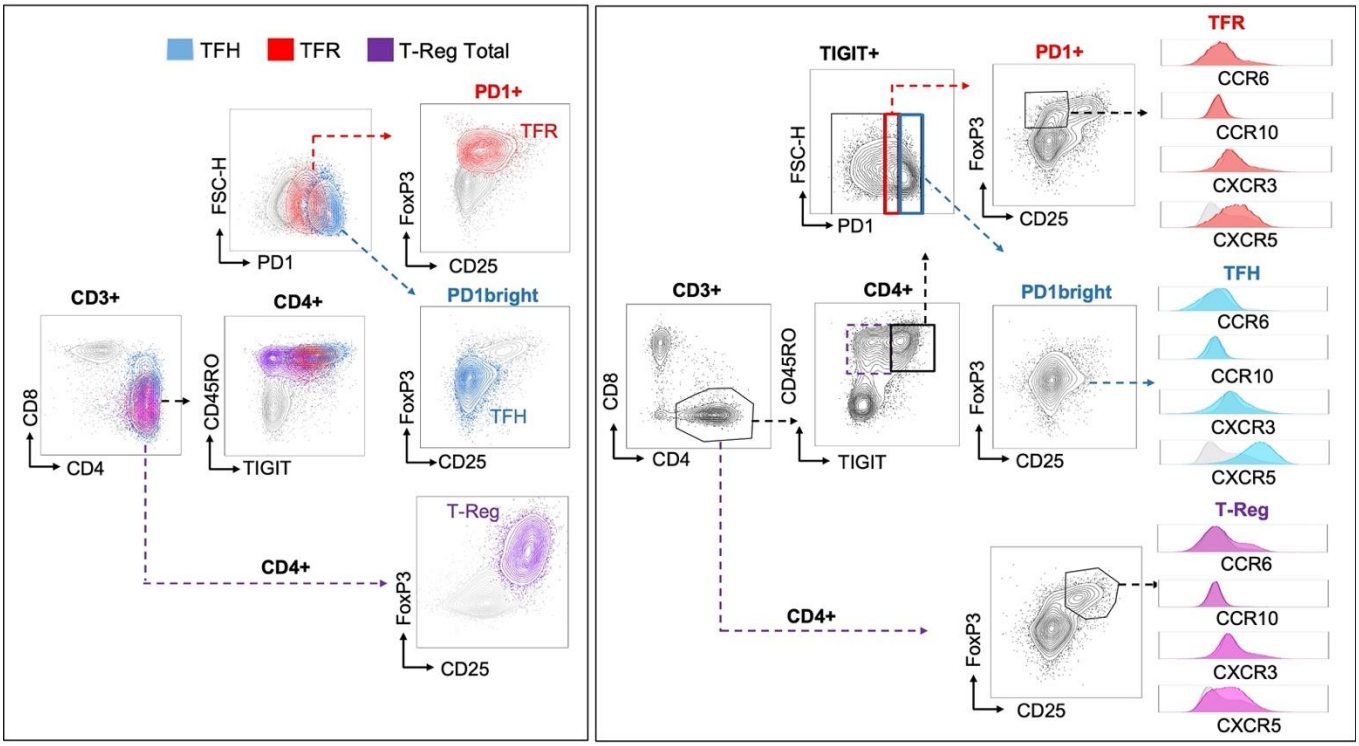

Figure S6. Additional characterization of TFH, TFR and T-regulatory cell (T-reg) populations. We utilized research panel II to further define the phenotype of populations identified by research panel I. Using a manual gating strategy, common markers between the research panels and the phenotype identified through computational analysis with research panel I, were used to identify TFH, TFR and T-Reg subpopulations in research panel II. These populations were further characterized by the expression of the chemokine receptors CCR6, CCR10, CXCR3, and CXCR5.

Supplementary Figure 7:

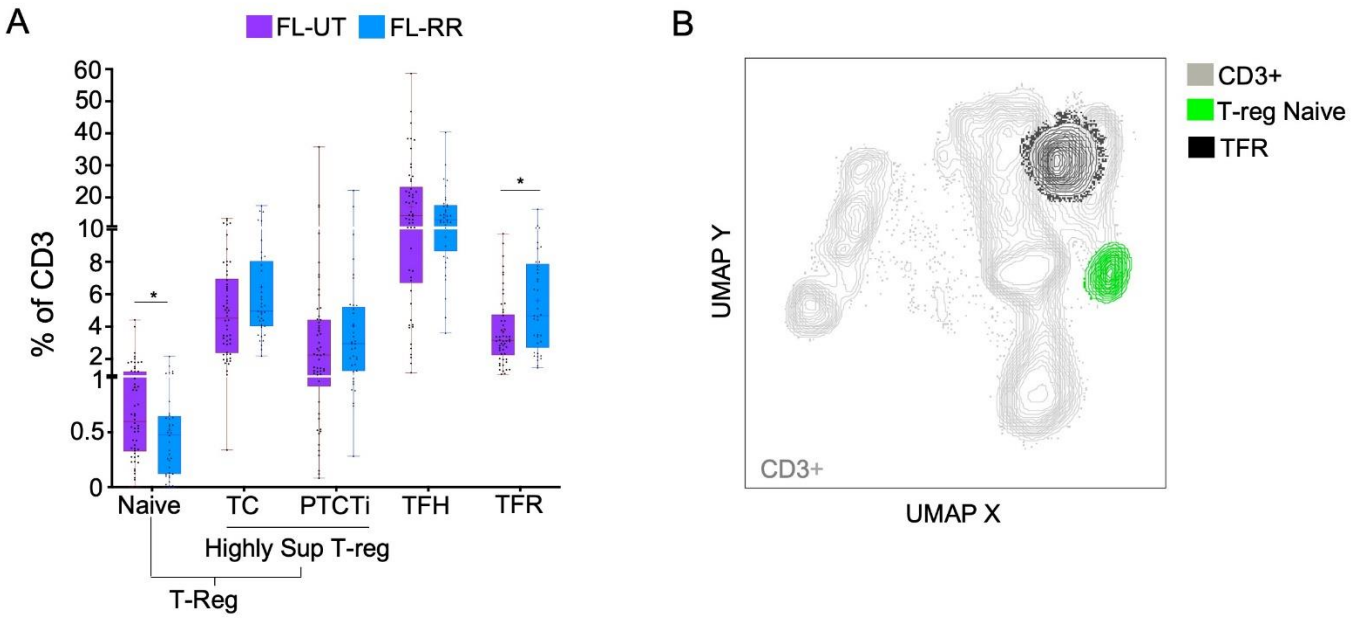

Figure S7. Alterations in FL-RR microenvironment in comparison to FL-UT. (A) Percentage of T-reg naïve, T-reg TC, Treg PTCTi, TFH and TFR in FL-UT and FL-RR. p- value *≤ 0.02. **(B)** Uniform Manifold Approximation and Projection (UMAP) of T-reg naïve and TFR in FL-UT and FL-RR.

Supplementary Figure 8:

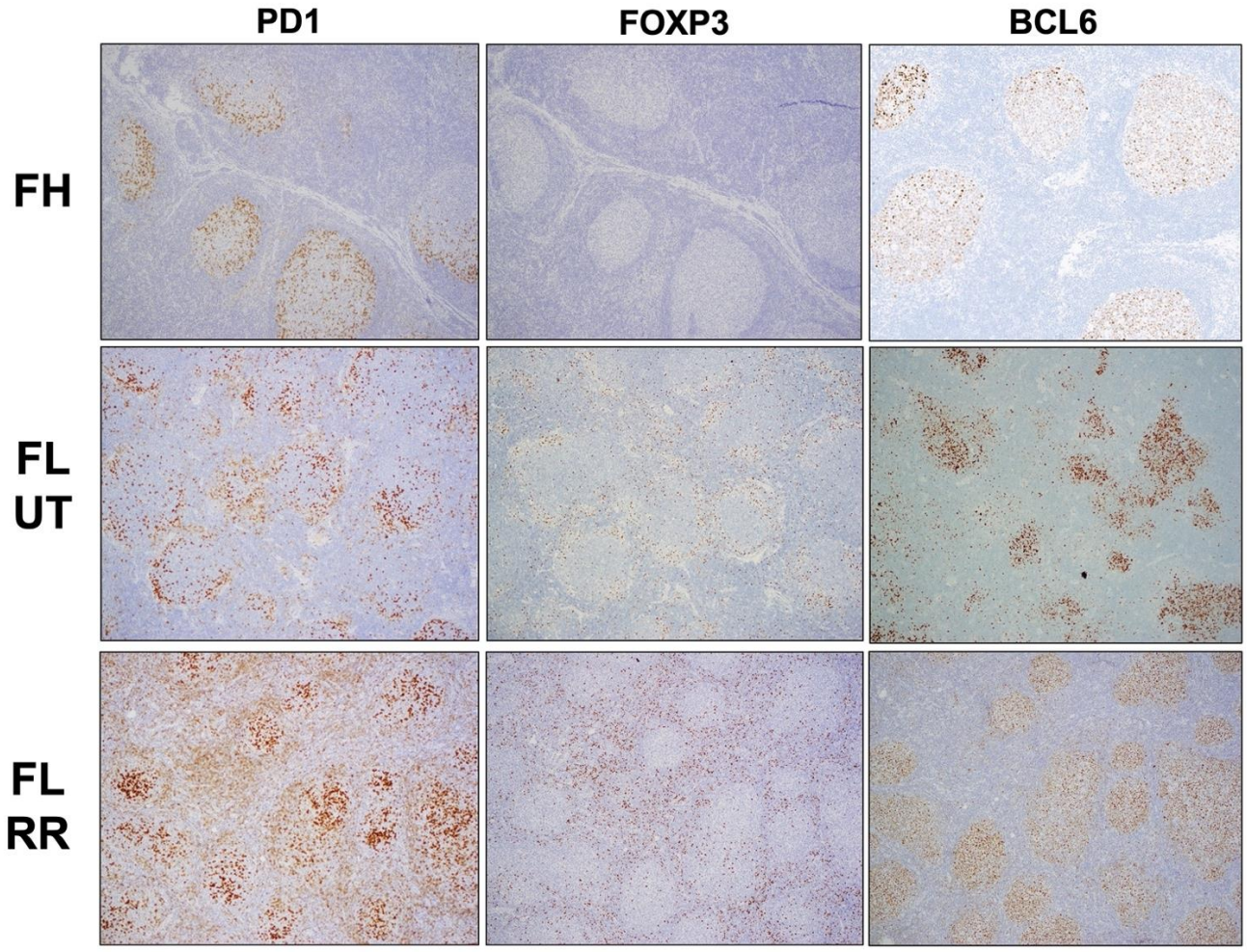

Figure S8. Immunohistochemical staining for PD1, FoxP3 and BCL-6 on reactive follicular hyperplasia (FH) and follicular lymphoma, untreated and relapsed/ refractory (FL-UT and FL-RR) specimens. In the FH specimen, PD1 brightly positive T-follicular helper cells (TFH) cells are present within the germinal centers and are polarized predominantly to the light zone. In the FL specimens, PD1 brightly positive TFH cells are seen within the neoplastic follicles and the dim PD1 positive, FoxP3 positive, BCL6 positive T-follicular regulatory cells (TFR) cells are seen within and surrounding the neoplastic follicles. Both TFH and TFR cells are present in higher density in both the FL specimens (FL-UT and FL-RR) vs FH specimen. TFR cells are present in a significantly higher frequency in FL-RR cases in comparison to both FH and FL-UT.

Supplementary Figure 9:

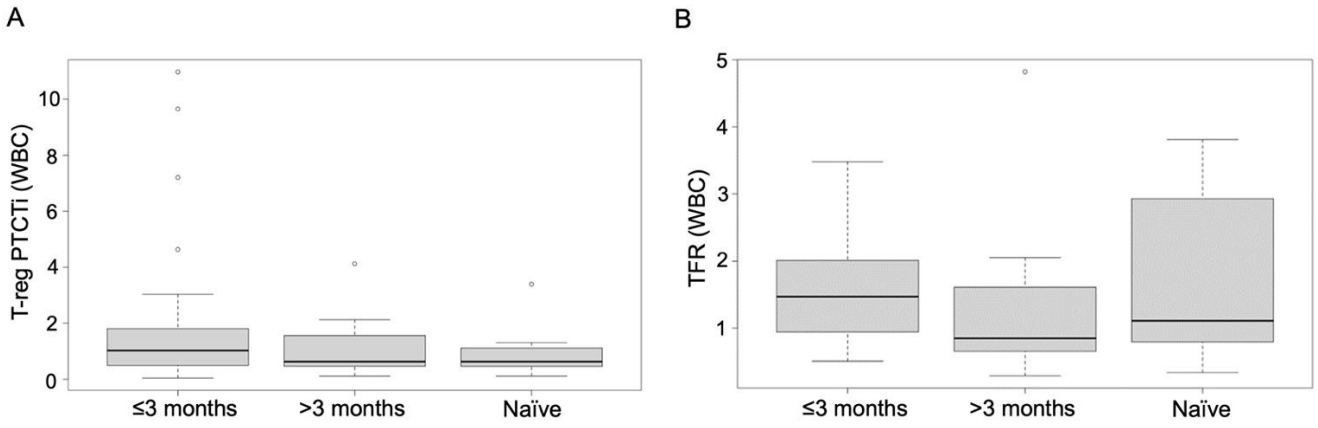

Figure S9. Correlation of T-reg PTCTi and TFR with earlier initiation of the therapy in FL-UT cohort. (A-B) T-reg PTCTi and TFR represented as percent of WBC plotted against time to first treatment (>3 months, <3 months).

Supplementary Figure 10:

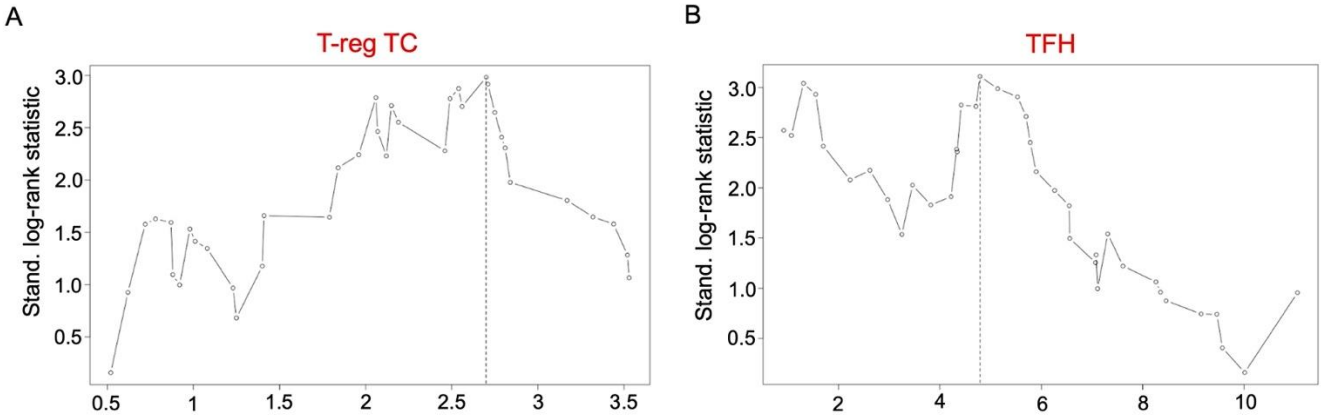

Figure S10. Maximally selected rank statistics on the FL-UT cohort. (A, B) Estimated optimal cutoff points for T-reg TC and TFH percentages are 2.7% and 4.79% of WBC, respectively.

Supplementary Figure 11:

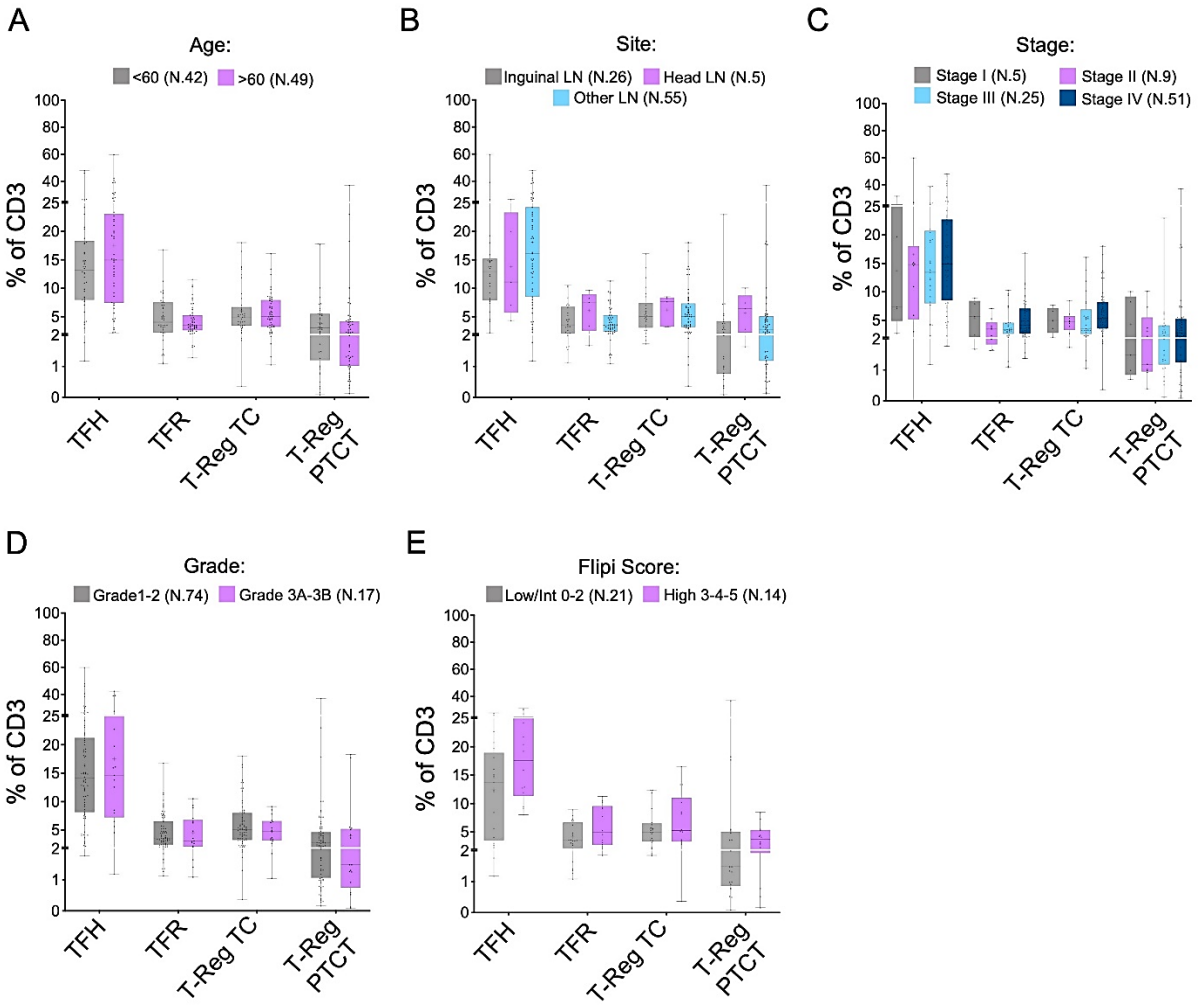

Figure S11. Distribution of immunosuppressive populations (T-reg TC, T-reg PTCTi and TFR) and TFH among various clinicopathological settings in both FL cohorts. (A) Age. (B) Site. (C) Stage. (D) Grade. (E) FLIPI score.

Supplementary Figure 12:

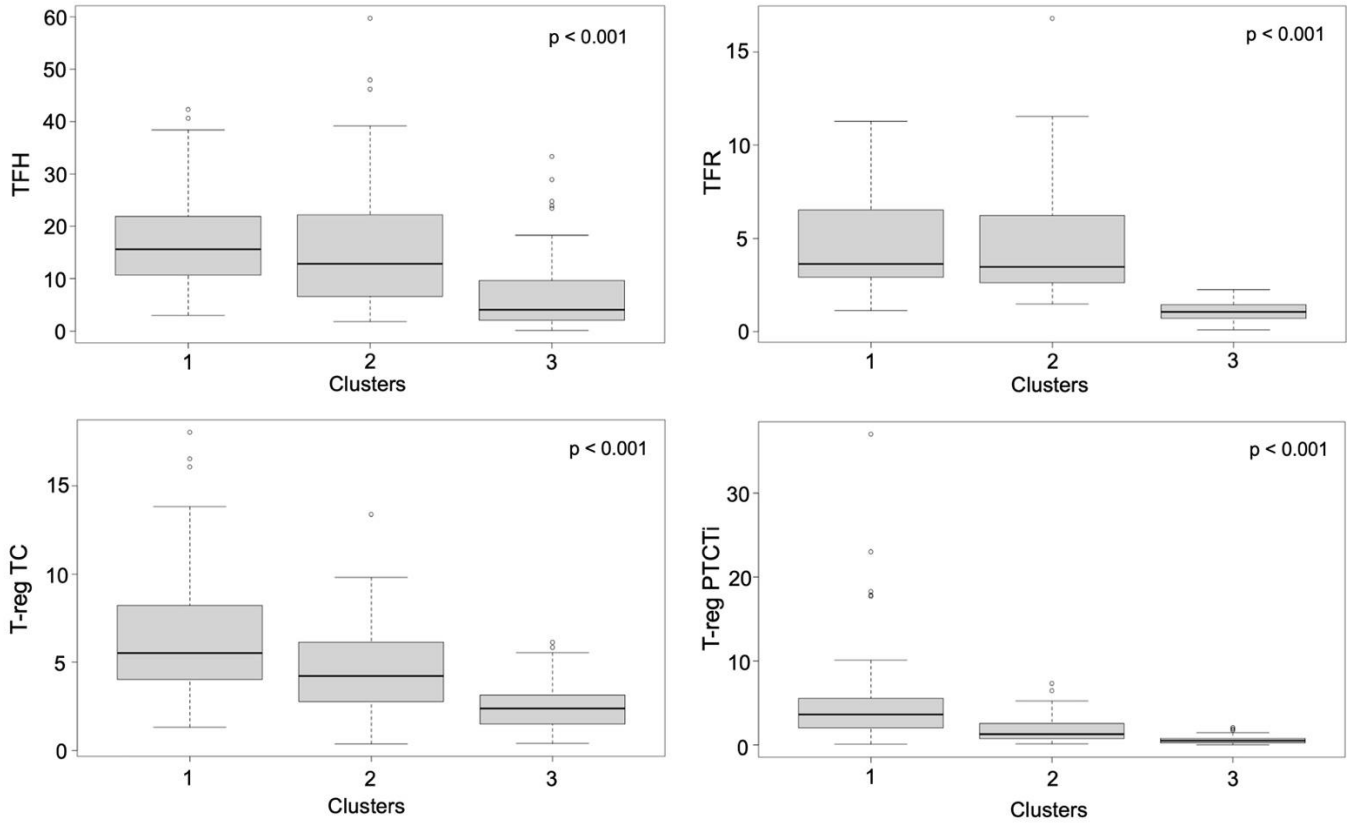

Figure S12. Distribution of T-cell subsets as percentage of WBCs in the 3 clusters identified by unsupervised hierarchical clustering that show statistical difference between the 3 clusters.

Supplementary Figure 13:

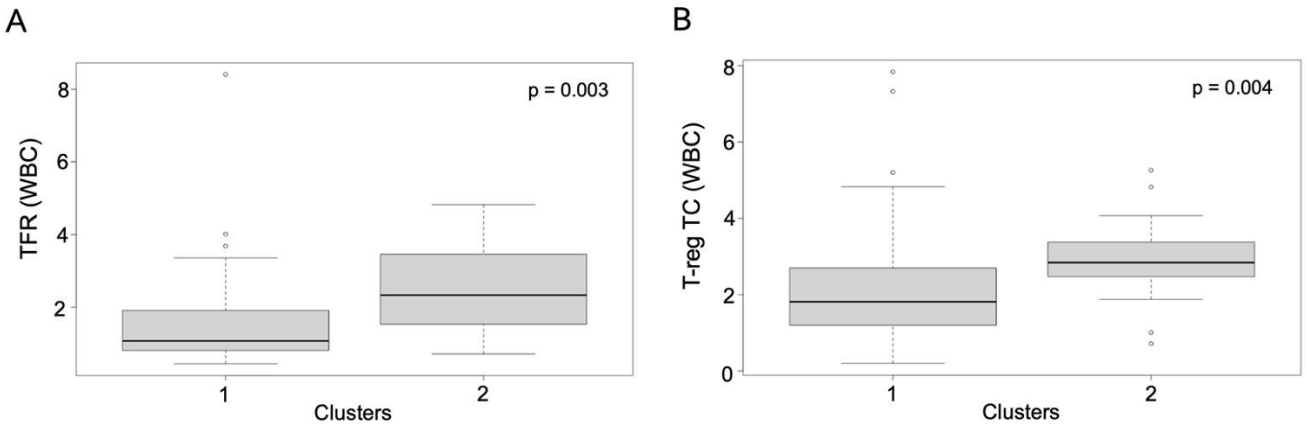

Figure S13. Distribution of T-cell subsets as percentage of WBCs in the clusters 1 and 2 (enriched in FL cases) that show statistical difference between the 2 clusters. (A) TFR. (B) T-reg TC.

Supplementary Figure 14:

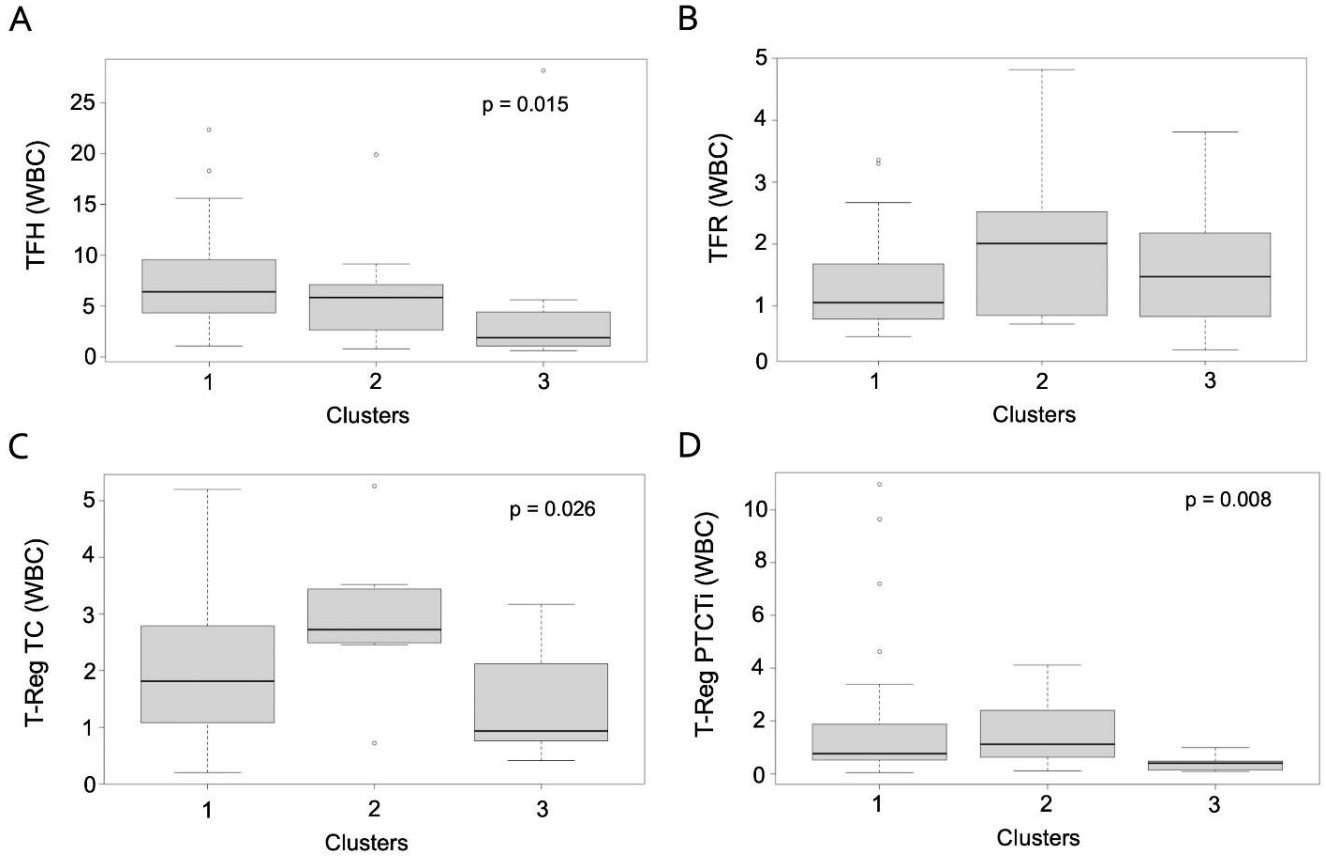

Figure S14: Distribution of T-cell subsets as percentage of WBCs in "FH-like FL" cases (10 FL-UT cases) in cluster 3 in comparison to other FL-UT cases present in clusters 1 and 2. (A) TFH. (B) TFR. (C) T-reg TC. (D) T-reg PTCTi.

Supplementary Figure 15:

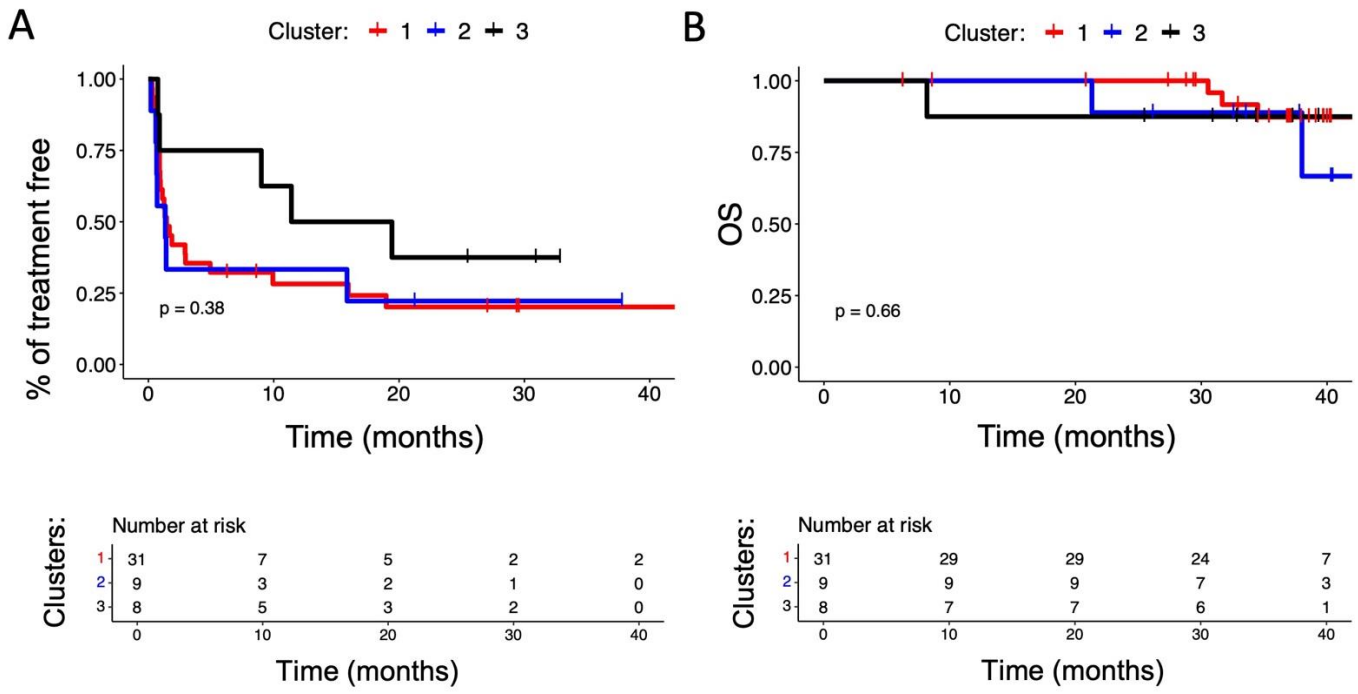

Figure S15. Kaplan Meier curve comparing FL-UT cases in cluster 1, cluster 2 and cluster 3 ("FH-like FL" cases). (A) Kaplan Meier curve illustrating time to first treatment of the FL-UT cases in cluster 1, cluster 2 and cluster 3 ("FH-like FL" cases) depicted in red, blue, and black curves, respectively. (B) Kaplan Meier curve illustrating overall survival of the FL-UT cases in cluster 1, cluster 2 and cluster 3 ("FH-like FL" cases) depicted in red, blue, and black curves, respectively.

Reference:

1. Hothorn T, Lausen B. On the exact distribution of maximally selected rank statistics. *Computational Statistics & Data Analysis*. 2003/06/28/ 2003;43(2):121-137.

Supplementary Tables

For Supplementary Tables from Table S1 to Table S9 please see separte Excel file